doi:10.1111/evo.13

Evolution of morphological integration in the skull of Carnivora (Mammalia): Changes in Canidae lead to increased evolutionary potential of facial traits

Fabio Andrade Machado,[1,2,3] Thiago Macek Gonçalves Zahn,[4] and Gabriel Marroig[4]

[1]*División Mastozoologa, Museo Argentino de Ciencias Naturales, "Bernardino Rivadavia". Av. Ángel Gallardo 470 (C1405DJR), Buenos Aires, Argentina*

[2]*Consejo Nacional de Investigaciones Científicas y Técnicas (CONICET), Buenos Aires, Argentina*

[3]*E-mail: macfabio@gmail.com*

[4]*Departamento de Genética e Biologia Evolutiva, Instituto de Biociências, Universidade de São Paulo, SP 05508-090, Brazil*

Received October 19, 2017
Accepted April 20, 2018

Morphological integration refers to the fact that different phenotypic traits of organisms are not fully independent from each other, and tend to covary to different degrees. The covariation among traits is thought to reflect properties of the species' genetic architecture and thus can have an impact on evolutionary responses. Furthermore, if morphological integration changes along the history of a group, inferences of past selection regimes might be problematic. Here, we evaluated the stability and evolution of the morphological integration of skull traits in Carnivora by using evolutionary simulations and phylogenetic comparative methods. Our results show that carnivoran species are able to respond to natural selection in a very similar way. Our comparative analyses show that the phylogenetic signal for pattern of integration is lower than that observed for morphology (trait averages), and that integration was stable throughout the evolution of the group. That notwithstanding, Canidae differed from other families by having higher integration, evolvability, flexibility, and allometric coefficients on the facial region. These changes might have allowed canids to rapidly adapt to different food sources, helping to explain not only the phenotypic diversification of the family, but also why humans were able to generate such a great diversity of dog breeds through artificial selection.

KEY WORDS: Covariance matrix, carnivora, canidae, modularity, morphometrics, P-matrix.

Morphological integration refers to the fact that different phenotypic traits of organisms are not fully independent from each other, and tend to covary to different degrees (Olson and Miller 1958). This pattern has long been noticed by students of anatomy such as Georges Cuvier, the father of paleontology, who recognized that parts were not only contingently associated with each other, but that they had to be in order for organisms to perform their specific functions (Cuvier and Jameson 1827). Although Cuvier concluded that integration (and its association with functional demands) was an impediment to the transmutation of species, Darwin later argued that correlations among traits should be understood as "laws of variation" arising from correlations of ontogenetic growth (Darwin 1859). In his view, integration is a constraint on the generation of variants, but not an absolute one, given that natural selection could ultimately overcome it in order to fine tune an species to its environment. Thus, the understanding of how populational variation is generated and how it interacts with natural selection in order to produce adaptations is a key component of evolutionary investigations (Lande 1979; Lande and Arnold 1983; Hansen and Martins 1996).

From a genetic perspective, covariation among traits is the product of pleiotropy and linkage disequilibrium (Falconer et al. 1996; Lynch et al. 1998; Hansen 2006). The covariation that arises from these factors influences not only how tightly related traits are in a population, but mainly how they will be inherited jointly (Hallgrímsson et al. 2009). This is especially important in the

context of the study of natural selection because, in the presence of genetic covariances, selection on a trait can indirectly influence the evolutionary response on other traits.

According to the multivariate breeder's equation (Lande 1979), the change in mean multivariate phenotype from one generation to the next will be

$$\mathbf{\Delta z} = \mathbf{G\beta} \tag{1}$$

where $\mathbf{\Delta z} = \{\Delta z_1, \Delta z_2, \ldots \Delta z_n\}$ is a column vector of mean changes in n traits; $\mathbf{G}$ is the nxn matrix of variance-covariance of additive genetic effects (e.g., elements G_{ii} are the additive genetic variances of trait i and elements G_{ij} are the additive genetic covariances between traits i and j), and $\mathbf{\beta} = \{\beta_1, \beta_2, \ldots \beta_n\}$ is the column vector of selection gradients, or the strength of selection acting on each trait (Lande 1979; Lande and Arnold 1983). To exemplify the importance of this concept, consider a system of two traits. For $\mathbf{\beta} = \{\beta_1, \beta_2\}$ the evolutionary response for each trait will be

$$\Delta z_1 = G_{11}\beta_1 + G_{12}\beta_2 \tag{2a}$$

$$\Delta z_2 = G_{21}\beta_1 + G_{22}\beta_2 \tag{2b}$$

Its easy to see that, in the presence of nonzero genetic covariances ($G_{12} = G_{21} \neq 0$), the evolutionary response of a trait will be a function not only of genetic variance and direct selection, but also of indirect selection and genetic covariance (Lande and Arnold 1983; Agrawal and Stinchcombe 2009; Marroig et al. 2011). This suggests that the investigation of species divergence (i.e., $\mathbf{\Delta z}$) alone can, at best, paint an incomplete picture of the evolutionary processes at work (see Grabowski 2016; Savell et al. 2016 for some empirical examples).

In comparative analysis, one of the main goals is to investigate past selective regimes in order to explain the observed diversity of forms. In a quantitative genetic framework, this is done by retrospectively estimating $\mathbf{\beta}$s from inferred $\mathbf{\Delta z}$s (e.g., Ackermann and Cheverud 2004; Marroig et al. 2004; Marroig and Cheverud 2005, 2010; Martínez-Abadías et al. 2012; Marroig et al. 2012; Schroeder et al. 2014; Grabowski 2016; Savell et al. 2016), which can be done by simply rearranging equation (1) as

$$\mathbf{\beta} = \mathbf{G}^{-1}\mathbf{\Delta z} \tag{3}$$

If $\mathbf{G}$ differs greatly between species, estimated $\mathbf{\beta}$s can be imprecise, leading to wrong conclusions about the evolutionary history of a group (Turelli 1988). So, to evaluate how well quantitative genetic theory can be applied in a macroevolutionary context, investigations about the similarity of morphological integration expressed in $\mathbf{G}$ among the species under study is a necessary first step.

The mammalian skull is an ideal model for the study of morphological integration in a comparative context. It is a complex structure made by the sum of simpler discrete units, or bones, which combine to form a larger integrated whole. The overall number and position of bones in the skull is remarkably conserved within mammals (Schoch 2006), allowing for a phylogenetically broader comparison of trait measurements (Pearson and Davin 1924). Even though each bone may be developmentally individualized, general ontogenetic factors affect more than one structure, producing different degrees of morphological integration and modularity (Cheverud 1982; Hall 2005; Hallgrímsson et al. 2007, 2009). Lastly, the skull is an important morpho-functional complex, combining diverse organs and functions that play important roles in species ecology and evolution (Cheverud 1982). Thus, differences in morphological integration impact how species will respond to natural selection, potentially affecting their evolutionary and ecological success.

Previous large-scale investigations of the morphological integration of the skull in mammals have painted a coherent picture. While matrices from different species respond similarly to natural selection (Marroig and Cheverud 2001; Oliveira et al. 2009; Marroig and Cheverud 2010; Shirai and Marroig 2010a; Haber 2016; Hubbe et al. 2016), magnitudes of overall integration (i.e. the strength of association between traits) tend to vary widely even between closely related species (Marroig and Cheverud 2001; Oliveira et al. 2009). Furthermore, modularity patterns seem conserved among the major mammalian clades (Goswami 2006a; Porto et al. 2009; Shirai and Marroig 2010a; Porto et al. 2013), reinforcing the idea that ontogenetic pathways and genetic architecture have been relatively stable throughout mammalian evolution. However, despite this stability at larger scales (Goswami 2006a; Porto et al. 2009, 2013), analyses within mammalian orders sometimes highlight differences in some species or genera (Oliveira et al. 2009; Shirai and Marroig 2010b; Hubbe et al. 2016) or even between families (Haber 2016). Thus, even though we expect that morphological integration will generally be conserved at broader scales, the investigation of less inclusive clades can still lead to significant insight into the evolution of morphological integration.

Here, we evaluate the stability (or absence thereof) of the patterns of morphological integration of the skull in Carnivoran mammals. Carnivores are one of the most species-rich clades of large Mammals, containing almost 300 extant species, and being the only order of mammals to have populated all continents on Earth, including Antarctica. Carnivora displays an impressive diversity of skull shape disparity (Radinsky 1981a, b, 1982; Drake and Klingenberg 2010), which is accompanied by an equally impressive diversity of feeding strategies, ecological specializations, and morphological variation. For these reasons, the group is considered to be an ideal natural model for the study of adaptation

in the macroevolutionary scale (Goswami 2010), especially regarding skull shape evolution (e.g., Wroe and Milne 2007; Christiansen 2008; Figueirido et al. 2009; Jones and Goswami 2009; Figueirido et al. 2010, 2011b, 2013; Slater et al. 2009, 2010a; Tseng and Wang 2011; Meloro et al. 2015; Tseng and Flynn 2015; Jones et al. 2015, Michaud et al. 2018). We aim to further the current knowledge of the evolution of morphological integration within Carnivora (e.g., Dayan et al. 2002; Meiri et al. 2005; Goswami 2006b) by using one of the most comprehensive datasets gathered to date in an explicit quantitative genetics context. We combine matrix comparison and phylogenetic comparative methods in order to **(1)** test the hypothesis of stability of patterns of skull trait covariance for Carnivora, **(2)** investigate which groups diverge, if any, and **(3)** describe any differences found.

Materials and Methods

SAMPLE, MORPHOMETRICS, AND PHYLOGENY

Over 8300 specimens from 17 institutions (see Acknowledgments for the list) have been examined. The removal of juveniles, specimens with uncertain taxonomic affinities, outliers, and species with insufficient samples produced a total of 6793 specimens (4442 Caniformes/2351 Feliformes) from 142 species (92 Caniformes/50 Feliformes) included in 81 genera (45 Caniformes/31 Feliformes), representing 15 carnivoran families (Prionodontidae being the only absent family). Additionally, we also included samples of *Canis familiaris dingo*, *C. lycaon,* and *C. rufus*, totaling 145 taxa (Table S2). See the Supporting Information for further information on Taxonomy, sample sizes, and outlier identification. A full list of specimen numbers is available upon request to the authors.

Phylogenetic relationships were compiled from a host of different sources (e.g., Arnold et al. 2010; Nyakatura and Bininda-Emonds 2012; Slater et al. 2012; Li et al. 2015; Figueiró et al. 2017; Zhou et al. 2017) producing a tree topology that best summarized current knowledge of phylogenetic relationships between species. Because some of the methods used here require a dated phylogeny, we estimated branch lengths via maximum-likelihood using cytochrome-B data downloaded from GenBank. A dated chronogram was produced by "congruifying" (*sensu* Eastman et al. 2013) the produced phylogram with Nyakatura and Bininda-Emonds (2012)'s dated supertree using the software PATHd8 (Britton et al. 2007). Species without available genetic information were later added to the dated phylogeny following information gathered from the literature. See Supporting Information for a full description of methods and sources. Results produced with different tree topologies (e.g., Bininda-Emonds et al. 2007; Agnarsson et al. 2010; Arnold et al. 2010; Nyakatura and Bininda-Emonds 2012) were consistent with those presented here (Figs. S16 and S17).

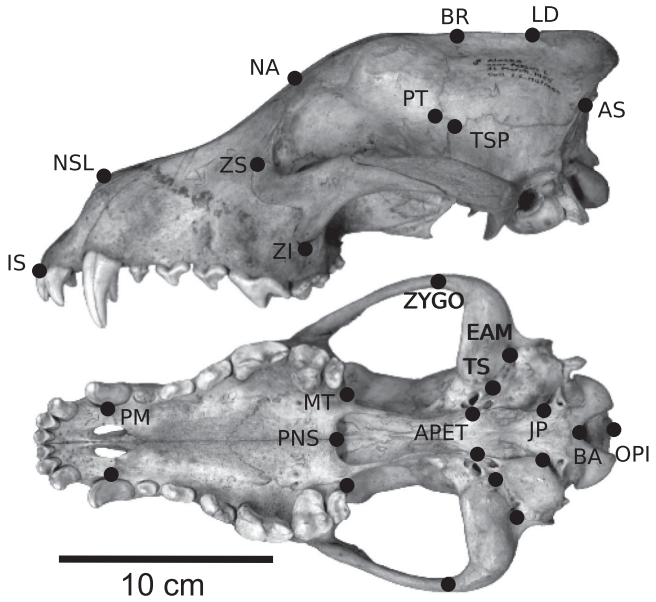

Figure 1. Anatomical Landmarks shown on the skull of a grey wolf (*Canis lupus*). Measurements are defined by the interlandmark distance between two points. See Table S1 for the full list of linear distances traits and their module membership.

The morphometric measurements were obtained through digitized anatomical landmarks of the skull (Fig. 1) with the aid of a Microscribe MLX system (Immersion Corporation, San Jose, California). Landmarking followed previous works from our research group (e.g., Cheverud 1982, 1996b; Ackermann and Cheverud 2000; Cheverud et al. 1983; Marroig and Cheverud 2001; Porto et al. 2009; Oliveira et al. 2009; Hubbe et al. 2016, Fig. 1). Skulls were digitized in two views to allow for the sampling of the whole skull. To unify these views, both configurations were mean-centered on the common landmarks and rotated in order to minimize their squared distances (Schönemann 1966). From the final configurations, we obtained a set of 35 interlandmark distances to describe the skull morphology, following Porto et al. (2009, Table S3). Bilaterally symmetrical measurements were averaged between sides when possible. Individuals were measured twice and repeatability was estimated following Lessells and Boag (1987). Repeatabilities were on average very high (Table S3) and thus measurements were averaged between replicates for downstream analyses.

Measurements (Table S1) were chosen to represent the size and shape of skull bones and structures in order to allow the quantification of local developmental, genetic, and functional processes (Pearson and Davin 1924; Cheverud 1982). Furthermore, the quantitative genetics of these measurements has been extensively studied and the similarity between genotypic and phenotypic variation/covariation patterns has been well established for multiple taxa (Porto et al. 2009; Marroig and Cheverud 2010;

Garcia et al. 2014; Porto et al. 2015), thus validating the so called "Cheverud Conjecture" (Cheverud 1988) for this set of traits. In other words, estimated phenotypic **P** matrices can be considered adequate models for the underlying **G** matrices.

Sources of variation that are not of interest for this investigation, such as geographical/subspecies variation, sexual dimorphism, age class, and captivity status (see Supporting Information for a description of these factors) were removed prior to the estimation of the phenotypic covariance matrices **P** using a multivariate linear model approach. The covariance matrix of the residuals of the linear model can be interpreted as the pooled within-groups covariance matrix. Table S2 shows the sources of variation controlled for in each species, and the Supporting Information explains the full procedure used for identifying relevant factors to be controlled for.

MATRIX COMPARISON

Covariance matrices were compared using the Random Skewers (RS) method (Cheverud 1996b; Cheverud and Marroig 2007). In RS, each matrix under comparison is multiplied by a set of randomly generated vectors (1000 in the present case), and each pair of response vectors is compared through vector correlation. The mean correlation between all pairs of vectors is taken as a similarity statistic between both matrices. Minimum samples sizes were obtained through rarefaction analysis following Goswami (2006b), according to which sample sizes of $n > 25$ were considered more similar to the full sample matrix than between-taxa comparisons (see Supplementary Information). Differences in sample sizes were accounted for using a Monte-Carlo matrix repeatability approach (Cheverud 1996b).

Rohlf (2017) has recently raised some questions regarding the RS method, namely the fact that it relies on the interpretation of average cosines/angles, a metric that might be difficult to interpret on its own (Rohlf, *pers. comn.*). However, many of the more problematic aspects of the distribution of cosines described in Rohlf (2017) were not observed for our sample, probably due to the fact that these patterns are restricted to low dimensionalities (Figs. S5 and S6), a context in which the use of RS is not advised to begin with (Marroig et al. 2011). Furthermore, for our sample, average cosines between responses were highly correlated with other parameters of the RS distribution (Fig. S7), supporting the classical interpretation of the RS metric (Cheverud and Marroig 2007; Hansen and Houle 2008; see Supplementary Information).

The use of RS can be further justified by the fact that it can be fully interpreted within the theoretical framework of quantitative genetics. Specifically, the skewers can be viewed as random selection gradients ($\boldsymbol{\beta}$) that are applied to a population with a genetic covariance matrix **G**, producing evolutionary responses $\boldsymbol{\Delta z}$, as in equation (1). Given that we are using **P** as a proxy for **G**, the use of RS can be interpreted as a measure of the capacity of different species to respond similarly to natural selection.

Because many of the methods used here require an Euclidean distance matrix of trait differences, we obtained an RS-derived distance based on Haber (2015), defined as $Dis_{RS} = \sqrt{2(1 - RS)}$, where RS is the matrix of pairwise RS similarities. We then performed a Principal Coordinate Analysis to investigate whether the resulting distance matrix was Euclidean. Eigenvectors (Pcoords) still associated with negative eigenvalues were excluded, and the remaining eigenvectors were used to describe the ordination of species in the "matrix-space" and to recalculate Dis_{RS}, which was used in downstream analyses.

Studies in the field of comparative quantitative genetics may use a variety of different matrix comparison techniques (e.g., Steppan 1997; Goswami 2006b; Marroig and Cheverud 2010; Blankers et al. 2017), which may provide different information regarding covariance structure, similarity, and dissimilarity (Haber 2015). However, most studies usually concentrate on a single method, hindering comparability between studies. For that reason, we verified our results using another metric, the Riemannian distance (Förstner and Moonen 1999; Mitteroecker and Bookstein 2009; Dryden et al. 2009), in an effort to improve comparability. The Riemannian distance between two positive-definite covariance matrices $\mathbf{P}_1$ and $\mathbf{P}_2$ is defined as

$$\|\mathbf{P}_1, \mathbf{P}_2\|_{cov} = \sqrt{\sum_{i=1}^{p} log(\lambda_i)^2} \tag{4}$$

where λ_i is the ith eigenvalue of $\mathbf{P}_1^{-1}\mathbf{P}_2$. Because some matrices had incomplete rank ($n < 35$), we reduced the dimensionality of our sample by projecting each **P** matrix on a common base, as follows:

$$\mathbf{P}_w = V'\mathbf{P}V \tag{5}$$

where V are the first five eigenvectors of the pooled covariance matrix for the whole sample (**W**).

This effectively reduces the dimensionality of the dataset to $k = 5$, ensuring not only that all matrices were positive-definite, but also that sample sizes were adequate, in accordance with Strauss (2010)'s "rule of thumb" of five specimens per dimension. As described above for Dis_{RS}, we performed a Principal Coordinate Analysis keeping only eigenvectors with positive eigenvalues to obtain an Euclidean distance between the species based on the Riemannian distance (Dis_{Ri}). To verify whether the procedure for obtaining Euclidean distances for the RS and Riemannian metrics resulted in significant loss of information, we calculated the correlation between Dis_{RS}/Dis_{Ri} and their corresponding original distance matrices.

Lastly, we obtained the magnitude of morphological integration as the average squared trait correlations ($\bar{r}^2$), which is a

measure of the overall intensity of association among traits. We performed a correlation analysis between $\bar{r}^2$ and each Pcoord in order to investigate if changes in overall integration among traits were responsible for a significant part of the variation in matrix structure.

MATRIX CORRELATION

To investigate whether differences in species' average morphology are related to differences in morphological integration, we performed a Linear Discriminant Analysis (LDA) on the data using species as a discriminant factor. The Euclidean distance between species on the LDA space is equal to the Mahalanobis (D) distance between groups and is a measure of morphological divergence that takes into account within-species variation (measured in this case as the pooled within-group variance-covariance). The relationship between the Mahalanobis distance D and Dis_{RS}/Dis_{Ri} can then be used to evaluate if morphological integration was influenced by evolution of the average phenotype (Marroig and Cheverud 2001; Oliveira et al. 2009). Furthermore, to investigate if changes in the magnitude of morphological integration can explain differences in covariance patterns (e.g., Oliveira et al. 2009) we obtained the matrix of Euclidean distances between species' $\bar{r}^2$ values ($Dis_{\bar{r}^2}$).

The comparison between Dis_{RS}/Dis_{Ri}, $Dis_{\bar{r}^2}$, and D was performed using matrix correlation, and the significance was assessed through permutation tests (Mantel 1967). We also calculated matrix partial correlations conditioning the variation of RS, $\bar{r}^2$ and D on a matrix of phylogenetic distances between species (Dow and Cheverud 1985; Marroig and Cheverud 2001) using the phylogenetic permutation procedure proposed by Harmon and Glor (2010).

PHYLOGENETIC SIGNAL AND DISPARITY THROUGH TIME

To investigate the tempo and mode of evolution of morphology (D), patterns (Dis_{RS}/Dis_{Ri}) and magnitude of integration ($Dis_{\bar{r}^2}$), we evaluated patterns of phenotypic evolution using Disparity Through Time (DTT) analyses and by calculating phylogenetic signals.

Phylogenetic signal was evaluated using the multivariate generalization of the K statistic (K-mult) proposed by Adams (2014) and implemented in the function *physignal* in the R package *geomorph* (Adams and Otárola-Castillo 2013). K-mult measures the phylogenetic signal as a deviation from the expected value under a Brownian Motion (BM) model of evolution (K-mult = 1) (Blomberg et al. 2003). Traits with K-mult value < 1 are more similar among distant relatives (and less similar among close relatives) than expected under BM, usually interpreted as more liable or convergent traits. On the other hand, traits with K-mult values > 1 are more similar between sister taxa, and less similar among distant relatives, than expected under BM, usually being interpreted as more conservative at the tips than at the base of the tree (Blomberg et al. 2003). The observed values for K-mult were tested against the null-distribution of no phylogenetic signal produced by permuting the tip labels of the phylogeny (Blomberg et al. 2003; Adams 2014).

The disparity through time (DDT) method is based on the calculation of the average within-clade disparity at the time of each cladogenetic event on a phylogeny (Harmon et al. 2003). Because at the origin of a group only one clade is present (the whole group), the average disparity at the base is equal to the total disparity for the group. Also, because at present time we only have tips, the average within-clade disparity drops to zero. If disparity is normalized as a ratio of total disparity, then plotting values against time produces a curve that goes from 1 at the origin of the group to 0 in the present. The empirical DTT curve produced was compared to a distribution of 1000 curves produced under a Brownian Motion evolutionary model by using the Disparity Index (MDI) proposed by Slater et al. (2010b), calculated with the *dtt* function in the R package *geiger* (Harmon et al. 2007). The MDI measures the area between the empirical curve and the median of the simulated curves. Positive values indicate that the empirical curve lies above the simulated ones, meaning that there is a high overlap between group phenotypes, a pattern usually interpreted as either a product of stabilizing selection (one peak Ornstein-Uhlenbeck model) or a "Late Burst" model (Edwards et al. 2015). Conversely, negative MDI values mean that the observed curve falls below the simulated ones, being consistent with an "Early Burst" model (Harmon et al. 2003). The difference in area between each simulated curve and the median was used as a null distribution of the BM model. Empirical values were compared to the distribution generated by simulation through a two-tailed test.

Because disparity for DTT is calculated as the Euclidean distance between species phenotypic values, calculations were performed on Dis_{RS}/Dis_{Ri}, $Dis_{\bar{r}^2}$ and D. The dated phylogeny was used for these analyses.

DIVERSITY DECOMPOSITION ANALYSIS

Because both phylogenetic signal and DTT analyses describe only broad patterns of phenotypic evolution, we also employed the diversity decomposition method (*decdiv*, Pavoine et al. 2010; Haber 2015) for morphology, patterns and magnitude of integration. This technique allows the decomposition of total trait diversity into the different nodes along a cladogram. Pavoine et al. (2010) also developed three specific tests based on this method. The first and second tests assess whether the observed pattern can be explained by differences in a single of just a few nodes, respectively. The third test verifies if trait divergence is skewed toward the root or the tips of the cladogram.

As this method requires an Euclidean distance matrix, tests were performed on Dis_{RS}/Dis_{Ri} (patterns of integration), Dis_{r^2} (magnitude of integration), and D (average phenotypic values), using the function *decdiv* (Supplementary Material of Pavoine et al. 2010). Significance was assessed through 999 permutations of the tip labels of the phylogeny. This method allows us to diagnose where in the evolutionary history of a group divergence is concentrated.

GROUP DIFFERENCES

Since our results strongly suggest that Canidae shows a difference in patterns of integration (see Results), we tested for differences between families in the matrix-space using pairwise nonparametric multivariate analyses of variance (NP-MANOVA, Anderson 2001; McArdle and Anderson 2001) over Dis_{RS} and Dis_{Ri}. Families with small species sample sizes ($n_s < 3$) were excluded in order to improve power for the remaining comparisons. Significance was obtained by 9999 permutations of the distance matrix (Anderson 2001), and *P*-values were corrected for multiple tests using the Bonferroni correction.

Additionally, we quantified multivariate overlap between families in the matrix space using a Monte Carlo technique initially proposed to study niche superposition (Swanson et al. 2015). This technique consists in modeling each group (family in the present case) using a multivariate normal distribution. Because this method requires good covariance estimates, we focused our investigation on the first two PCoords of Dis_{RS} and Dis_{Ri}, and on families with larger species sample sizes ($n_s > 5$). This led to the exclusion of monotypic families, Eupleridae, Hyenidae, and Ursidae. For the remaining families, Monte-Carlo samples (1000 observations) were generated using the modeled distributions, and overlap was calculated as the proportion of observations that fall within the 95% multivariate ellipsoid of other families. Uncertainty is evaluated in a Bayesian framework by obtaining a posterior of multivariate normals for each family (1000 samples) using a flat prior, as suggested by Swanson et al. (2015). The procedure is then repeated for each element of the posterior distribution.

Pairwise NP-MANOVAs were performed with the package *RVAideMemoire* (Hervé 2016) and multivariate overlap was measured using the package *nicheROVER* (Lysy et al. 2014).

MODULARITY

We tested all species for the modularity hypotheses proposed by Porto et al. (2009, 2013) for mammals, including Carnivora. This was done by building "hypothetical matrices": that is trait by trait matrices containing 1s for all entries within modules and 0s for all other entries (Cheverud 1995, 1996b). Each covariance matrix was then transformed into its correlation counterpart, and the correlation between those matrices and the hypothetical ones was calculated by taking the Pearson product-moment correlation between the lower triangle of both matrices. Since the entries in a correlation matrix are not independent data points, null distributions were constructed through 999 permutations, and the null-hypothesis of no pattern was rejected if the correlation was greater than 95% of the randomly generated values (Cheverud 1982).

Following Porto et al. (2009) we tested the Oral, Nasal, Zygomatic, Vault, and Base cranial module hypotheses as well as hypotheses representing the two main cranial regions—Face and Neurocranium (Table S1). Additionally, we also tested composite hypotheses including more than one module/region, produced by summing different hypothetical matrices and setting all values larger than 1 to 1. Specifically, we used two composite hypotheses: "Total," including all modules, and "Neuroface," which evaluates both cranial regions jointly. Because families showed different rates of rejection of the null hypothesis of no modularity (see Results), we also investigated whether individual families differed from the full sample in their rate of rejection, using $\chi - square$ tests. $P - values$ from the $\chi - square$ tests were corrected for multiple comparisons using the Bonferroni correction.

CHARACTERIZATION OF VARIATION IN MORPHOLOGICAL INTEGRATION

In order to describe the observed variation in covariance structure associated to the axes (Pcoords) of matrix space with biologically meaningful variables (Rohlf 2017), we obtained a series of evolutionary and modularity-related measures.

We calculated the AVG ratio (Cheverud 1995, 1996a; Marroig et al. 2004) for all modularity hypotheses (see above). The AVG ratio is calculated as the ratio between the average correlation of traits within a given hypothetical module (AVG+; 1s in the hypothetical matrix) and the average correlation among other traits and between modules (AVG–; 0s in the hypothetical matrix). If this ratio is higher than 1, this means that the traits inside a module are more integrated than those outside and between modules. If the value is lower than 1, then the within-module correlations are lower than those outside the module. Comparing the AVG ratios of different modules between groups with dissimilar covariance structures allows one to identify whether the differences in covariance structure are related to increased (or decreased) correlations in particular regions of the skull.

To investigate the potential evolutionary consequences of observed differences in morphological integration, we measured flexibilities and evolvabilities for each species. Flexibility expresses the capacity of a species to respond in the direction of natural selection, and is measured as the vector correlation between the selection gradient $\boldsymbol{\beta}$ and the evolutionary response $\boldsymbol{\Delta z}$ (Marroig et al. 2009). Evolvability quantifies the amount of

variation available in the direction of natural selection and is measured as the projection of $\mathbf{\Delta z}$ onto $\boldsymbol{\beta}$ (Hansen and Houle 2008).

These statistics are usually given as global indexes to evaluate the overall capacity of a population to evolve in all directions of phenotypic space (e.g., Marroig et al. 2009), and are measured as the average value for a set of randomly generated $\boldsymbol{\beta}$ ($\bar{f}$ and $\bar{e}$). However, because $\bar{f}$ closely tracks the value of $\bar{r^2}$ (Pearson's $r = -0.935$ for the present case), and because $\bar{e}$ depends on the overall species size for unscaled measurements (Pearson's $r = 0.940$, using the log geometric mean of measurements as size and $\log \bar{e}$), the utility of such global indexes to identify small changes in covariance patterns between groups may often be limited. Here, we focus on estimating flexibilities and evolvabilities in specific directions instead (f and e, respectively, Hansen and Houle 2008; Garcia et al. 2014), namely in the direction of individual traits. This can be seen as a way to investigate the capacity of each trait to respond individually in the direction of selection (Garcia et al. 2014), and was used to identify whether each region of the skull displays differences in evolutionary ability without making prior assumptions about modularity.

For calculations of f and e we first produced $\boldsymbol{\beta}$s consisting of 1 for a given trait and 0 for all others. Each trait-specific $\boldsymbol{\beta}$ and its resulting $\mathbf{\Delta z}$ were then used to obtain both statistics for each trait. Because evolvability of unscaled traits increases with species size (Marroig et al. 2009), estimated values were scaled by the matrix trace, and thus evolvabilities are given as proportions of total variance. Evolvabilities calculated in this way are equal to the proportion that each character contributes to the total variance. The resulting $\mathbf{\Delta z}$ based on this $\boldsymbol{\beta}$ is equal to the line/column of the covariance matrix containing the nonzero trait (eq. 2). Thus, the vector correlation between selection and response (f) is a way to assess how the covariances of each trait can impact evolutionary potential.

Lastly, we investigated if observed changes in covariance patterns were associated with shifts in static allometry. For the mammalian skull, allometric size variation is usually expressed on the first principal component (PC1) of the covariance matrix, which contains loadings with the same direction for most traits (Porto et al. 2013). Allometric size variation is thought to be an important constraint to the evolution of multivariate traits, biasing the direction of evolution and acting as a "line of least evolutionary resistance" (Marroig and Cheverud 2010). Changes in allometry were assessed/evaluated using individual trait loadings on each species' PC1 (i.e., regression slopes between each trait and the underlying size factor, Jolicoeur 1963).

To observe how these variables relate to changes in **P** matrix structure, the resulting statistics (AVG ratios, f, e and allometric coefficients) were correlated to the first two axes of variation of the matrix-space (PCoords of Dis_{RS}/Dis_{Ri}; (Haber 2015)). Because the magnitude of integration is thought to covary with various aspects of morphological integration (Porto et al. 2009; Marroig et al. 2009), we computed semi-partial correlations between the PCoords and the statistics above holding $\sqrt{\bar{r^2}}$ fixed. This was done in order to evaluate if changes along a PCoord could be described more parsimoniously as a shift in overall integration, rather than multiple shifts in individual AVG ratios, fs, es or allometric coefficients. *P*-values for multiple tests were adjusted using the Bonferroni correction.

Results

MATRIX COMPARISON

The full table of 10,440 pairwise Random Skewers comparisons for all 145 taxa is available at the Supporting Information (Fig. S8). Observed and corrected RS values were highly correlated (Pearson's $r = 0.993$) and results of comparative analyses were similar with both. Henceforth we focus on the results using observed values.

The Principal Coordinate Analyses of the Riemannian and RS-based distances produced 88 and 108 positive eigenvalues, respectively. The Euclidean distance matrices obtained from these Pcoords (Dis_{RS}/Dis_{Ri}) had a high and significant correlation with their corresponding original distance matrices (Pearson's $r = 0.997$ and 0.992 for Dis_{RS} and Dis_{Ri}, respectively), suggesting that the PCOA did not result in a significant loss of information.

Figure 2A and B displays the first two PCoords for both RS and Riemannian distances. The first two axes jointly explain, respectively, 21.39 and 45.53% of the total variation. The overlap between families on both matrix-spaces was extensive, with the exception of the first PCoord for the RS-based distance and the second PCoord (Fig. 2A) for the Riemannian distance (Fig. 2B). On both these axes, canids have lower values, showing no (RS) or little (Riemannian) overlap with other families (Fig. 2). Specifically, the dingo (*Canis familiaris dingo*) is placed at extreme negative values of the aforementioned axes. The matrix correlation between Euclidean distances calculated on both subspaces was considerably high, especially when comparing fewer dimensions of these spaces (e.g., cor = 0.601, 0.642, and 0.704 for 88, 6, and 2 Pcoords, respectively).

Regarding the distribution of $\bar{r^2}$ (Fig. 2C), overlap was great among families, with Procyonidae, Viveridae, Hyaenidae, and Herpestidae showing the lowest values and Ursidae and Odobenidae showing the highest. Canidae had low to intermediate values, with dingoes falling on the upper bound of the distribution.

PHYLOGENETIC SIGNAL, DISPARITY THROUGH TIME, AND DIVERSITY DECOMPOSITION

A significant phylogenetic signal was found for all variables investigated, with morphological integration (Dis_{RS} and Dis_{Ri}) showing

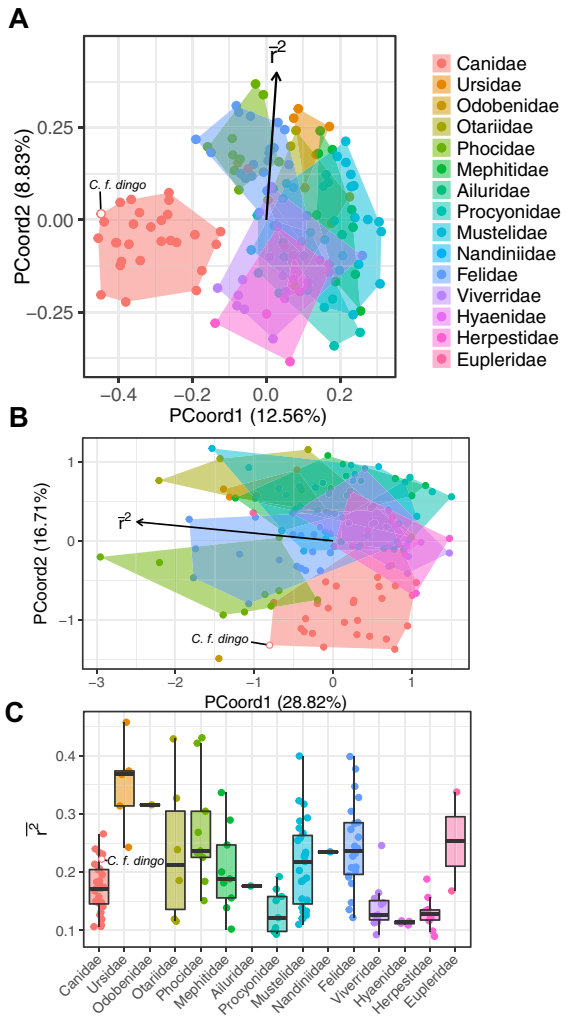

Figure 2. First two axes of the principal coordinate analysis of Dis_{RS} (A) and Dis_{Ri} (B) and overall morphological integration ($\bar{r}^2$) (C) for different Carnivora families. *C. f. dingo-Canis familiaris dingo*.

the lowest value of K, magnitude of integration ($\bar{r}^2$) presenting intermediate values and morphology (LDA) showing the highest K (Table 1). All MDI values were positive and significantly different from the BM simulations (Table 1). The evolution of the average disparity through time was also distinct among variables (Fig. 3). While patterns of integration (Dis_{RS} and Dis_{Ri}) showed large values of disparity throughout the group's evolution, only declining abruptly at the tips, magnitude of integration ($Dis_{\bar{r}^2}$) evolved consistently with BM at the beginning of the evolution of the group, only later presenting values above the BM simulations. Morphology (D) showed average disparities almost constantly slightly above the expected by BM. Accordingly, all MDI values were positive and significant, with the ones for patterns of integration being the highest, magnitude of integration again at an intermediate value, and morphology showing the lowest value (Table 1).

Table 1. Phylogenetic signal (K-mult), morphological disparity index (MDI) and statistic for diversity decomposition analysis (decdiv) for patterns of morphological integration (RS/Riemann), magnitude of integration ($\bar{r}^2$), and morphology (LDA).

	RS	Riemann	$\bar{r}^2$	LDA
K-mult	0.136*	0.141*	0.170*	0.495*
MDI	0.478*	0.443*	0.371*	0.151*
decdiv				
Single	0.266*	0.107*	0.131*	0.237*
Few	0.541*	0.350*	0.584*	0.696*
Root-skewness	0.795*	0.652*	0.670*	0.845*

Single—Test of the hypothesis that diversification is concentrated in a single node. Few—Test of the hypothesis that diversification is concentrated in few nodes. Root skewness—Test of the hypothesis that diversification is skewed either toward the tips (negative values) or the root (positive values). Asterisks indicate significant results at $\alpha = 0.05$.

The results of the permutation tests of the Diversity Decomposition analysis rejected the null hypotheses for all tests (Single node, Few nodes, and Root skewness), for all variables (Table 1). This result is expected when most of the diversification is concentrated in a few nodes at the base, with one node contributing most of the variation (Pavoine et al. 2010). The amount of diversity explained at each node for Dis_{RS} and Dis_{Ri} was highly correlated (Pearson's $r = 0.940$), and visually nearly identical (Fig. 4A and B). Overall, patterns of integration seem to show less diversification toward the tips, with large shifts concentrated at the origin of some clades, mainly at the node leading to Canidae and Arctoidea. Magnitude of integration seems to be slightly more dispersed over the phylogeny, despite still being more concentrated at the base. The largest shifts seem to be associated with the divergence of Ursidae from other Arctoidea and the divergence of Felidae from other Feliformia (Fig. 4C). For morphology, the signal is dominated by a single large shift concentrated at the divergence of Pinnipedia from Musteloidea (Fig. 4D).

GROUP DIFFERENCES AND MATRIX CORRELATION

The pairwise MANOVA tests show that, overall, Dis_{RS} had higher discrimination rates, showing a larger number of significant differences between families than Dis_{Ri} (Table 2). Regardless of the metric used, Canidae differs significantly from all other families, as was the case for Felidae and Mustelidae in the analysis using Dis_{RS}.

Regarding the multivariate overlap analysis on Dis_{RS} (Table 3A), while almost all families show high overlaps (> 50%) with at least two other families, Canidae consistently showed the smallest values (< 5% overlap with all other families). Additionally, the overlap of other families *with* Canidae was equally small

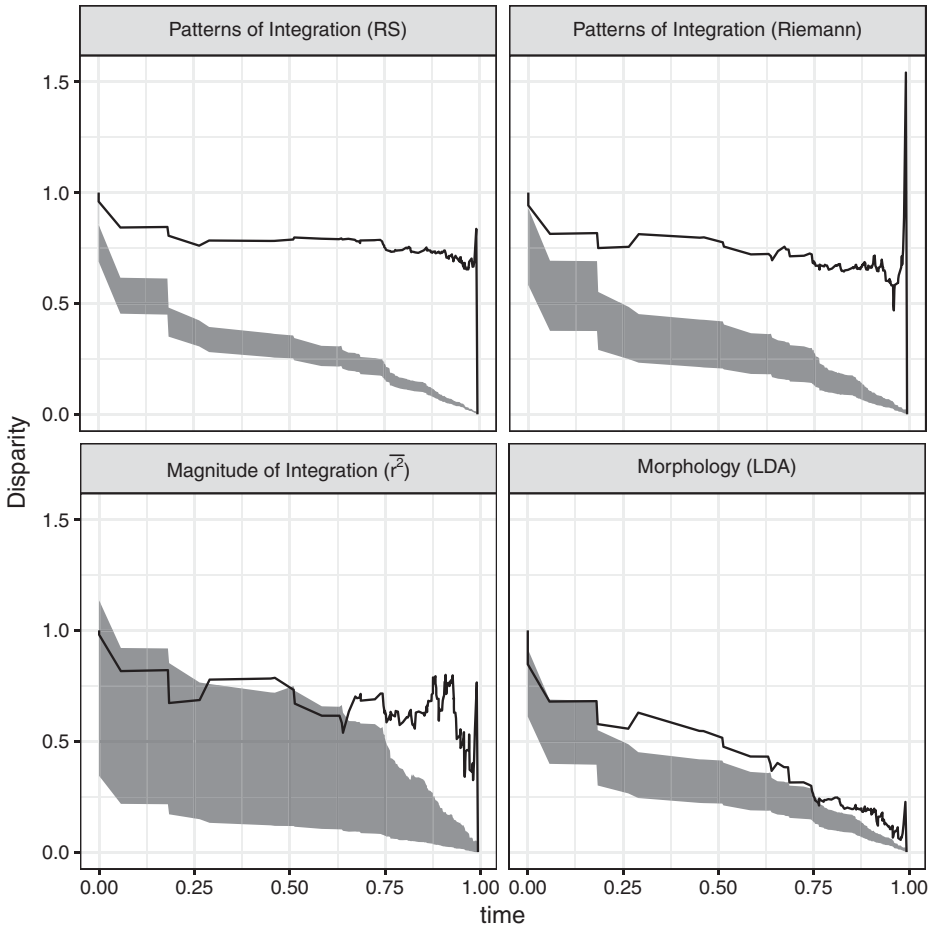

Figure 3. Disparity through time plots for integration patterns ($Dis_{P\,coord}$), magnitude of integration ($Dis_{\bar{r}^2}$) and morphology as measured by LDA (D). Gray envelopes represent the 95% confidence intervals for the null hypothesis of neutral (Brownian motion) evolution. Time shown is relative from the root of the phylogeny (0.00) to the present (1.00).

(< 5%). Generally speaking, Canidae showed the smallest average overlap of the sample: 0.014, contrary to other families that show values > 0.266.

The analysis with Dis_{Ri} shows higher overlap between groups: all families have high overlaps (> 50%) with at least four other families, except for Canidae, which shows high overlap only with Phocidae (Table 3B). All families had average overlaps of 0.45–0.65, except once again for Canidae, which had the lowest average overlap among all families (0.268). Even when Canidae presented a substantive overlap with another family (e.g., Phocidae, Mephitidae), that family never presented high or moderate overlap with Canidae (Table 3B). In fact, overlap *with* Canidae was systematically low (< 20%) for all families but Herpestidae.

The matrix correlations between Dis_{RS}/Dis_{Ri} and both $Dis_{\bar{r}^2}$ and D were significant, the correlation between Dis_{Ri} and $Dis_{\bar{r}^2}$ being the highest (Table 4). Partial correlations conditioned on the phylogenetic distances between species were very similar to their standard correlation counterparts.

MODULARITY

The results for the modularity tests can be seen in Table S8. Modularity was statistically significant ($P < 0.05$) mainly for the Nasal and Oral hypotheses, with rejection of the null hypothesis in 67.4 and 77.1% of all species, respectively. The Zygomatic module was largely undetected, with the exception of a few canids, otariids, procyonids, and hyenids, totaling only 4.2% of the species. The Base and Vault modules were not detected in any taxon. The Face region was detected in almost all instances (91.7%), while the Neurocranium was detected in none. Regarding composite hypotheses, NeuroFace was detected in almost all species (97.9%) while the Full hypothesis was detected in a few (34.7%). At the family level, the results seem to be consistent with the overall pattern, with the Oral module being detected in the majority of cases, followed by the Nasal and then the Zygomatic. The only clear exception seems to be Canidae, where the Nasal module was detected in all species (100% of species), followed by the Oral module (88.9% of species). $\chi - square$

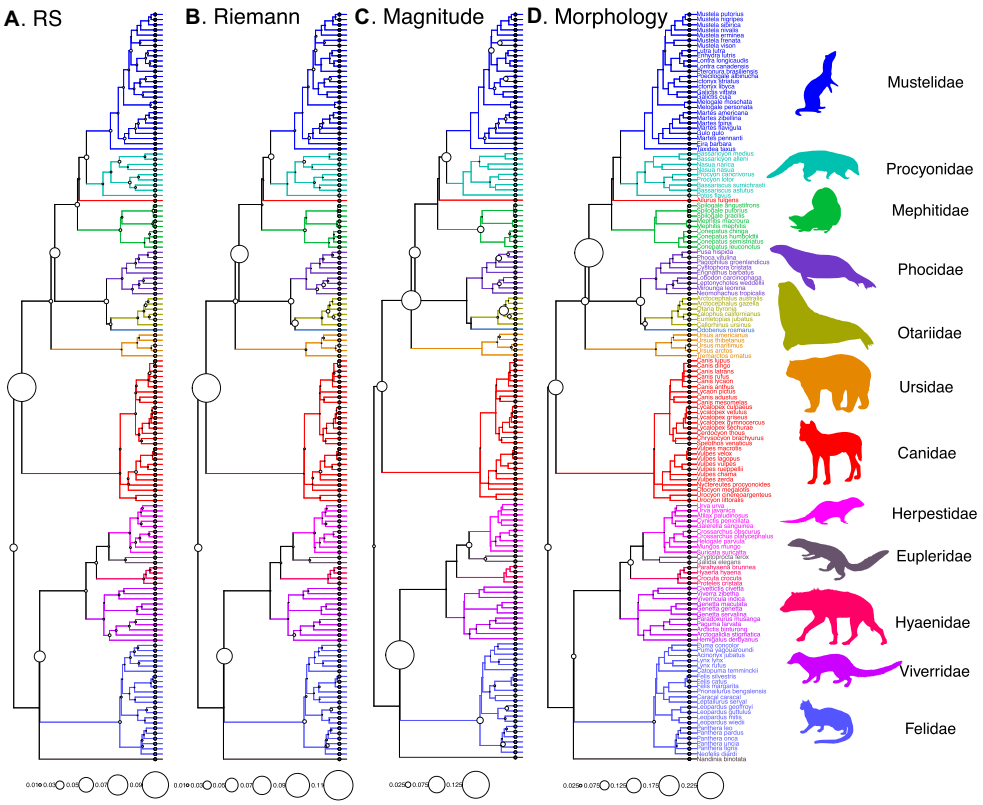

Figure 4. **Results of the diversity decomposition analysis. The size of the circles is proportional to the percentage of the total diversity explained by each node. (A) Patterns of morphological integration as represented by the first 108 PCoords of Dis_{RS}. (B) Patterns of morphological integration as represented by the first 88 PCoords of Dis_{Ri}. (C) Magnitude of integration measured by $\bar{r}^2$. (D) Variation in morphology measured by LDA (D). Monotypic families (*Ailurus fulgens, Odobenus rosmarus,* and *Nandinia binonata*) were not represented with a silhouette.**

tests for similarity of proportions showed, however, that after correction for multiple tests no family deviated from what was expected for the full sample ($P > 0.1$ for all tests), including the Nasal and Oral modules for Canidae ($P = 0.103$ and 1.000, respectively).

CHARACTERIZATION OF VARIATION IN MORPHOLOGICAL INTEGRATION

Even though the matrix-spaces defined by Dis_{RS} and Dis_{Ri} were not identical, as mentioned above the first two PCoords concentrated a significant part of the variance for both metrics (Fig. S9). Furthermore, the first PCoord of Dis_{Ri} has a high and negative correlation with the second PCoord of Dis_{RS} (Pearson's $r = -0.92$), and likewise PCoord2 of Dis_{Ri} is highly correlated with PCoord1 of Dis_{RS} (Pearson's $r = 0.899$).

Correlation analyses with PCoord1 of Dis_{RS} and PCoord2 of Dis_{Ri} show that lower scores are associated with increased flexibility, evolvability, and allometry in traits belonging to both Nasal and Oral modules, along with a reduction of evolvability and allometric coefficients associated with Base traits (Figs. 5 and 6). Some Zygomatic traits show a decrease in both evolvability and allometric coefficients, while some traits in the Vault show increased flexibility, but reduced evolvability and allometry associated with lower PCoord1 (Dis_{RS}) or PCoord2 (Dis_{Ri}) values (Figs. 5 and 6). Additionally, lower scores in these PCoords are associated with higher AVG ratios for the Nasal module and lower values for the Neurocranial region (Table S4). Semipartial correlations controlling for the variation in $\bar{r}^2$ did not differ from the standard correlation results.

For the PCoord2 of Dis_{RS} and the PCoord1 of Dis_{Ri}, correlation analyses show that these axes are associated with integration changes throughout the skull (Tables S4 to S7 and Figs. S10 and S11). In fact, these two axes were the only ones significantly correlated to $\sqrt{\bar{r}^2}$ (Pearson's $r = -0.928$ and 0.891, respectively). Actually, when we account for the variation in $\sqrt{\bar{r}^2}$, all semipartial correlations with these axes are rendered nonsignificant (Tables S4 to S7). Thus, these axes can be seen mostly as representing variation in $\bar{r}^2$, and all changes in flexibility, evolvability, AVG ratios, and allometry associated with them are therefore probably related to changes in overall integration.

Table 2. *P*-values of the NP-MANOVA pairwise tests.

	1.Can	2.Urs	3.Ota	4.Pho	5.Mep	6.Pro	7.Mus	8.Fel	9.Viv	10.Hya	11.Her
1.Canidae		**0.006**	**0.006**	**0.006**	**0.006**	**0.006**	**0.006**	**0.006**	**0.006**	**0.006**	**0.006**
2.Ursidae	**0.006**		0.077	**0.028**	**0.044**	0.055	**0.006**	**0.006**	**0.028**	0.479	**0.022**
3.Otariidae	**0.006**	1.000		**0.033**	**0.017**	**0.011**	**0.006**	**0.006**	**0.006**	0.259	**0.011**
4.Phocidae	**0.006**	**0.028**	**0.028**		**0.006**	**0.006**	**0.006**	**0.006**	**0.006**	0.066	**0.011**
5.Mephitidae	**0.006**	0.825	1.000	**0.017**		**0.006**	**0.006**	**0.006**	**0.006**	0.094	**0.011**
6.Procyonidae	**0.006**	**0.033**	0.209	**0.006**	0.528		**0.011**	**0.006**	**0.011**	0.154	**0.028**
7.Mustelidae	**0.006**	0.083	0.935	**0.006**	1.000	0.055		**0.006**	**0.006**	**0.011**	**0.006**
8.Felidae	**0.006**	0.924	0.385	**0.006**	**0.017**	**0.022**	**0.006**		**0.006**	**0.006**	**0.006**
9.Viverridae	**0.006**	**0.011**	**0.044**	**0.011**	**0.011**	0.341	**0.011**	**0.006**		0.110	0.649
10.Hyaenidae	**0.006**	0.803	1.000	0.083	0.094	0.209	**0.050**	**0.050**	1.000		0.528
11.Herpestidae	**0.006**	**0.022**	0.077	**0.006**	0.055	1.000	**0.039**	**0.006**	1.000	1.000	

Values below the diagonal are based on the Riemaniann distance (Dis_{Ri}) and values above the diagonal are based on the RS distance (Dis_{RS}). Bold values are significant at $\alpha < 0.05$.

Table 3. Analysis of multivariate overlap showing proportion of generated observations from one family (each row) falling within the 95% confidence ellipsoid of another family (columns).

A.RS	1.Can	2.Ota	3.Pho	4.Mep	5.Pro	6.Mus	7.Fel	8.Viv	9.Her	*Average*
1.Canidae		*0.000*	*0.023*	*0.010*	*0.000*	*0.007*	*0.007*	*0.036*	*0.031*	0.014
2.Otariidae	*0.000*		0.847	0.9275	0.2935	0.568	0.866	0.685	0.026	0.527
3.Phocidae	*0.014*	0.452		0.7765	0.3835	0.724	0.831	0.872	0.266	0.540
4.Mephitidae	*0.007*	0.573	0.83		0.219	0.469	0.836	0.818	0.079	0.479
5.Procyonidae	*0.000*	0.089	0.55	0.263		0.876	0.497	0.619	0.150	0.381
6.Mustelidae	*0.005*	0.145	0.71	0.389	0.756		0.619	0.740	0.352	0.465
7.Felidae	*0.004*	0.544	0.89	0.847	0.450	0.730		0.826	0.142	0.554
8.Viverridae	*0.019*	0.329	0.80	0.670	0.300	0.645	0.710		0.342	0.476
9.Herpestidae	*0.037*	0.020	0.38	0.115	0.187	0.634	0.161	0.598		0.266

A.Riemann	1.Can	2.Ota	3.Pho	4.Mep	5.Pro	6.Mus	7.Fel	8.Viv	9.Her	*Average*
1.Canidae		0.069	0.847	0.467	*0.013*	0.077	0.363	0.22	0.085	0.268
2.Otariidae	*0.032*		0.890	0.831	0.283	0.376	0.658	0.629	*0.020*	0.465
3.Phocidae	0.169	0.624		0.778	0.335	0.453	0.658	0.627	0.115	0.470
4.Mephitidae	0.098	0.653	0.812		0.204	0.325	0.610	0.682	0.072	0.432
5.Procyonidae	*0.007*	0.333	0.798	0.691		0.807	0.685	0.761	0.113	0.524
6.Mustelidae	0.062	0.464	0.952	0.882	0.827		0.888	0.906	0.321	0.663
7.Felidae	0.161	0.698	0.981	0.946	0.461	0.712		0.898	0.225	0.635
8.Viverridae	0.107	0.605	0.919	0.906	0.436	0.632	0.825		0.220	0.581
9.Herpestidae	0.436	0.082	0.852	0.613	0.437	0.778	0.688	0.781		0.583

Values are the median (50% quantile) overlaps found for the posterior distribution of multivariate normals. Italic - median overlap < 5%. Light gray cells- median overlap > 10%. Dark gray cells- median overlap > 20%. Black cells- median overlap > 50%.

Discussion

EVOLUTION OF MORPHOLOGICAL INTEGRATION

The stability of genetic covariance structure is a usually underevaluated premise of studies on the evolution of multivariate traits. Without its evaluation, the fact that traits covary in an evolutionary context cannot be attributed to selection or genetic constraints, much less is it possible to gauge the relative contribution of each factor (Felsenstein 2004; Marroig and Cheverud 2010). Here, we sought to investigate this premise through the comparison of phenotypic **P** matrices of skull measurements among species of Carnivora in an explicit quantitative genetics framework. The analysis of matrix similarity through Random Skewers (RS) showed that, despite not being identical, the matrices have high similarity values (Fig. S8). These values were as high as the ones observed among Old World Monkeys (Oliveira et al. 2009), Xenarthrans (Hubbe et al. 2016), and Ruminants (Haber 2015), but lower on

Table 4. Standard and partial correlations between dissimilarity matrices of patterns of morphological integration (Dis_{RS}/Dis_{Ri}) and both magnitude of integration differences ($Dis_{\bar{r}^2}$) and Mahalanobis distance (D).

	Standard		Partial	
	Dis_{RS}	Dis_{Ri}	Dis_{Ri}	Dis_{RS}
$\bar{r}^2$	0.268*	0.674*	0.674*	0.261*
D	0.278*	0.399*	0.379*	0.211*

Partial-correlations were calculated conditioning the relationship between both matrices on a matrix of phylogenetic distance. *- significant at $\alpha < 0.05$.

average than what was observed for New World Monkeys (Marroig and Cheverud 2001). However, the average similarity within less inclusive taxa such as families is higher in comparison to that found in New World Monkeys and within Ruminant families. In fact, the similarity among different families is comparable to that seen both between suborders of primates (Porto et al. 2009) and between Ruminant families (Haber 2016), suggesting that patterns of morphological integration are as conserved within Carnivora as they are within other orders of eutherian mammals (Goswami 2006a; Porto et al. 2009).

Nevertheless, different analyses presented here consistently showed that Canidae has the most divergent covariation pattern among all Carnivora. The diversity decomposition analysis showed that morphological integration patterns diverged early in the history of Carnivora (Table 1), mainly in association with the divergence of Canidae (Fig. 4). The nonparametric MANOVAs and multivariate superposition analyses pointed to the divergence of Canidae as relevant (Tables 3 and 2), suggesting that, even though other groups vary in their integration patterns, the observed range of variation overlaps among higher taxa (Fig. 2).

The evolution of morphological integration in the Carnivoran skull has been investigated mainly in two previous works. While Meiri et al. (2005) evaluated cranial measurements directly (e.g., length, height), their main findings were related to variation and covariation of teeth morphology, and its relationship to diet (see also Dayan et al. 2002). Goswami (2006b), on the other hand, explicitly evaluated morphological integration using 3D geometric morphometrics, and found that, despite the high similarity among groups, there was some phylogenetic and ecological patterning in morphological integration, with less inclusive taxa being more similar among themselves than more inclusive ones. Although we also found the presence of significant phylogenetic signal (multivariate Bloomberg's K) for morphological integration, its value was small and subclade average disparity (as revealed by DTT) was high throughout the evolution of the group (Tables 1 and 3). While low phylogenetic signal and stable subclade average disparity suggest an Ornstein–Uhlenbeck (OU, Hansen 1997) model of evolution, the divergence of Canidae and the DTT profile (Fig. 3) suggest a two-peak OU model (see Supporting Information and Fig. S18). Taken together with high RS values, these results point to the conclusion that, except for the initial divergence of Canidae (PCoord2 for Dis_{Ri} or PCoord1 for Dis_{RS}) and the variation attributed to changes in magnitude of integration (PCoord1 for Dis_{Ri} or PCoord2 for Dis_{RS}), the morphological integration structure was mostly stable along the evolution of Carnivora. While this does not negate the influence of ecology in modifying morphological integration, as pointed by Meiri et al. (2005) and Goswami (2006b), it does suggest that internal constraints impose a stronger influence in shaping the covariance structure (Cheverud 1982, 1984). This implies that the same basic covariance structure can produce a wide range of average morphologies aligned with distinct ecological demands. This is further reinforced by the fact that all Carnivora investigated here, including Canidae, share modularity patterns common to all therian mammals (Goswami 2006a; Porto et al. 2009, 2013), implying that ontogenetic pathways are conserved throughout this group. The fine-tuning of these ontogenetic pathways would result in internal stabilizing selection (Cheverud 1984) that would ultimately impose a similar covariance structure on different species, independent of average morphology (Lande 1980), thus helping explain the observed stability.

Previous works have shown that the overall magnitude of integration is a key aspect of morphological integration, and that changes in magnitude can deeply impact how species potentially respond to natural selection (Marroig et al. 2009; Porto et al. 2013; Haber 2016). Matrix correlation analyses here show that the association between patterns and magnitudes is significant for Carnivora (Table 4), despite being lower than the one observed for Catharrini (Oliveira et al. 2009). Nevertheless, the shift in patterns of integration in Canidae does not seems to be accompanied by a large shift in $\bar{r}^2$ (Fig. 4). Furthermore, the divergence of Canidae on the matrix-space (along Pcoord1 for Dis_{RS} or PCoord2 for Dis_{Ri}) seems to be nearly orthogonal to the divergence in $\bar{r}^2$. Thus, while changes in magnitudes can account for some variation in the patterns of integration, they cannot account for the main shift observed at the origin of Canidae.

Despite the stability in morphological integration, average morphology itself (henceforth referred to as "morphology" for brevity) evolved in a more complex manner. Phylogenetic signal for average morphology was higher than that observed for integration, showing values closer to those expected under Brownian motion (Table 1). However, despite its small value, the MDI was significantly different from that expected under BM, suggesting that this model is not enough to account for the morphological evolution of the group. This pattern could be

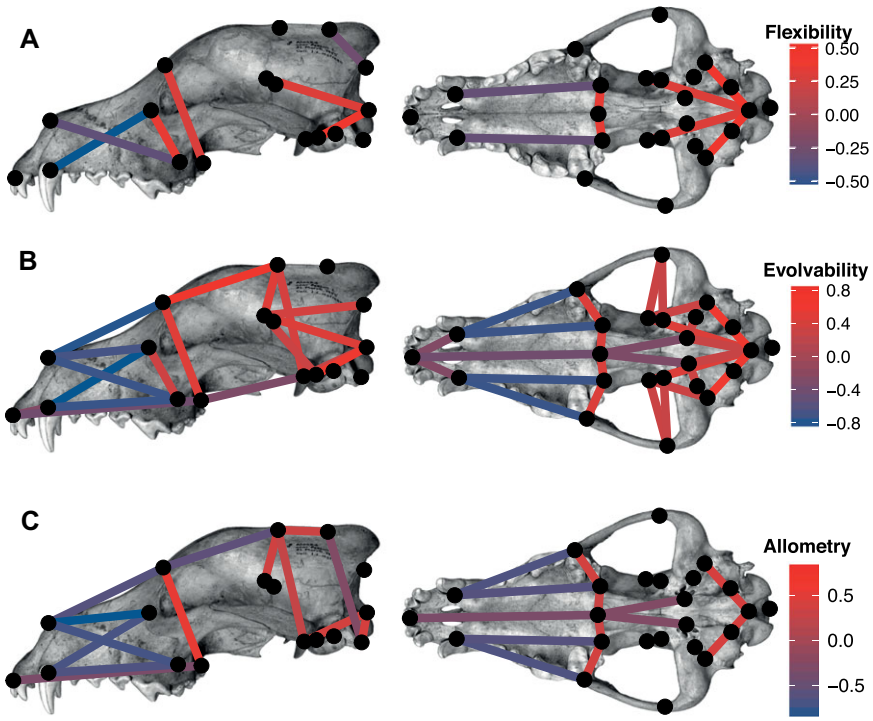

Figure 5. Graphical representation of the correlation analysis of trait-specific statistics on the skull of *Canis lupus*. Colors are proportional to the correlation values with PCoord1 of the space defined by Dis_{RS}. Nonsignificant correlations were omitted. (A) Flexibility in the direction of individual traits; (B) Evolvability in the direction of individual traits (i.e., relative variance of each trait). (C) Allometric coefficients for individual traits.

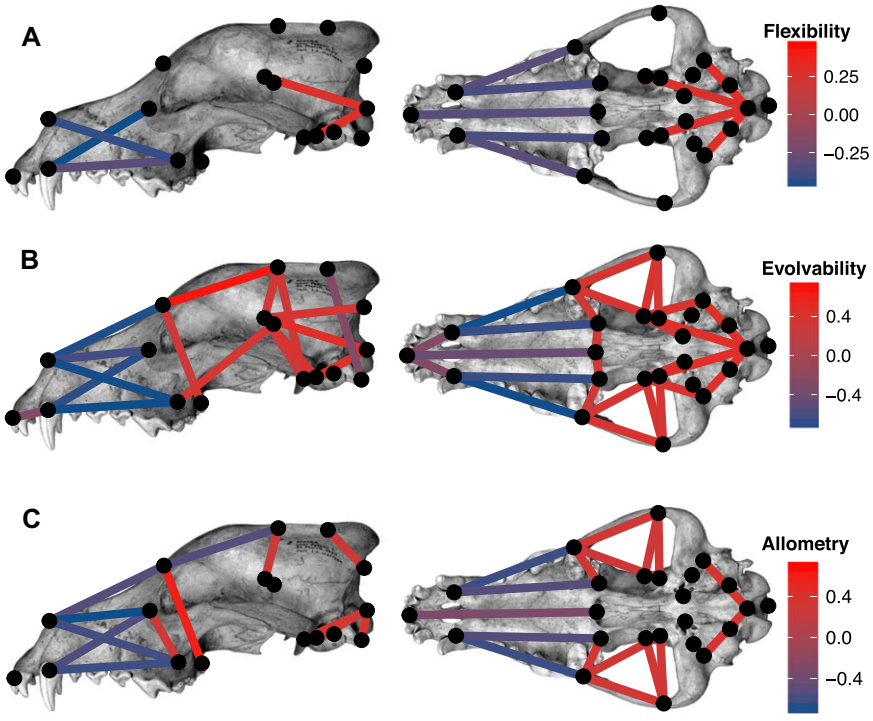

Figure 6. Graphical representation of the correlation analysis of trait-specific statistics on the skull of *Canis lupus*. Colors are proportional to the correlation values with PCoord2 of the space defined by Dis_{Ri}. Nonsignificant correlations were omitted. (A) Flexibility in the direction of individual traits; (B) Evolvability in the direction of individual traits (i.e., relative variance of each trait). (C) Allometric coefficients for individual traits.

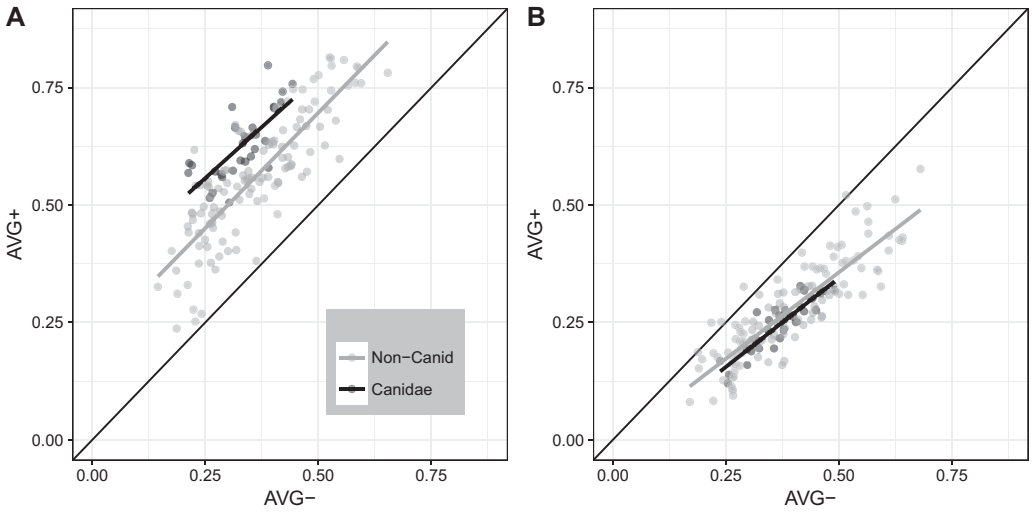

Figure 7. Relationship between AVG+ and AVG– for the Nasal module (A) and the Neurocranium region (B). Dashed black line represents AVG+ = AVG–. Solid trend lines are linear fits for the data.

achieved by the presence of high levels of phylogenetic structuring (or "inertia") of morphology at more inclusive levels, such as between families (Radinsky 1981a, 1981b, 1982; Figueirido et al. 2011a; Dumont et al. 2016), with subsequent within-family ecomorphological adaptations (Mattson 1998; Sacco and Van Valkenburgh 2004; Figueirido et al. 2009; Jones and Goswami 2009; Slater et al. 2009, 2010a; Meloro et al. 2014; Kienle and Berta 2015) or between-group convergence (Gaubert et al. 2005; Figueirido et al. 2010; Tseng and Wang 2011; Figueirido et al. 2011b, 2013; Dumont et al. 2016).

Some association between morphology and morphological integration has been observed here even when we account for phylogenetic relatedness (Table 4), suggesting that both factors might be coevolving along the history of Carnivora. However, the signal for this association is weak and seems to arise largely due to the large shift in morphology at the origin of Pinnipedia (Fig. 4C), as evidenced by the decrease in correlation between morphology and integration with the removal of this group (Partial Matrix correlation = 0.136/0.056, $P = 0.012/0.149$ for Dis_{Ri} and Dis_{RS}, respectively). Thus, while the origin of Pinnipedia might be associated with shifts in both integration and morphology, on a broader scale species averages seem to be evolving mostly independently of patterns of integration, similarly to what was observed for New World Monkeys (Marroig and Cheverud 2001).

Even though this is one of the first formal tests of stability of covariance patterns using modern comparative methods, we should stress that, while these methods and models have a strong theoretical evolutionary foundation (Hansen and Martins 1996; Felsenstein 2004), their application on variational properties, instead of averages, is not fully developed or understood. So, while we expect that multivariate stabilizing selection would produce an OU-like pattern in "matrix space," neither the demonstration that this is actually the case nor the description of such a space (but see Garcia et al. 2016) are currently available. Here, we employed two distinct metrics, one *structural* or *geometric*, consistent with the mathematical description of the space of covariance matrices and considered the "natural" distance between covariance matrices, the Riemannian distance (Förstner and Moonen 1999; Dryden et al. 2009; Mitteroecker and Bookstein 2009; Bookstein and Mitteroecker 2014), and the other based on evolutionary or *functional* aspects of the genetic additive covariance matrix, the Random Skewers method (Cheverud and Marroig 2007; Hansen and Houle 2008; Haber 2015). Both methods were consistent in pointing to divergence in Canidae, suggesting not only the existence of differences in morphological integration structure, but also that these imply differences in how species with these structures respond to natural selection. However, the results for both metrics differed in various details, ranging from the specific values of comparative statistics to the relative importance of overall integration on covariance patterns. Future works should expand on these topics to build an integrative view of the macroevolution of morphological integration.

CANIDAE

Our analysis has shown that Canidae modularity patterns are similar to those of the rest of Carnivora, and thus changes in modularity cannot explain the observed shifts in morphological integration for this group. This is not surprising, given that previous works have shown that modularity patterns are conserved throughout eutherian mammals (Goswami 2006a; Porto et al. 2009), and that Canidae in general and *Canis familiaris* specifically share the same modularity pattern as the remaining Carnivora (Drake and

Klingenberg 2010). The identified differences, however, seem to be enough to significantly alter how Canidae potentially responds to natural selection.

The investigation of correlations of PCOA axes (PCoords) with trait-based (evolvability, flexibility, and allometric coefficients) and modularity statistics (AVG ratios) revealed that the distinction between Canidae and the remaining Carnivora is largely due to changes in facial (Oral and Nasal) traits. For Canidae, traits expressing the length of the snout show an increase in flexibility (alignment of Δz and β, Figs. 6 and 5A), evolvability (amount of variation in the direction of selection β, Figs. 6 and 5B) and allometric coefficients (slope of the regression of each trait on size, Figs. 6 and 5C). Additionally, integration among Nasal traits is actually higher in Canidae than in other Carnivora, as shown not only by the presence of higher AVG ratios for this region (Table S4), but also by the fact that these higher values arise from increased correlation among facial traits (AVG+, Fig. 7, S12 and S13). In other words, while facial traits are more integrated among themselves, traits representing the relative length of the face display a larger variance and, thus, increased capacity to respond to natural selection. Changes in the neurocranium region and the zygomatic module were also observed, although they were less evident (Figs. 6, 5, and 7).

This pattern can be partly explained by the fact that these traits have higher allometric coefficients in canids than in other Carnivora (Figs. 6 and 5C). An increased association with size would lead to larger correlations among traits and possibly to larger variances, given that size is usually the main source of morphological variation in mammals. Because size is thought to constrain and bias the direction of multivariate evolution (Marroig and Cheverud 2010; Simon et al. 2016), increased facial allometry will ensure that most evolutionary responses will lead to larger changes in facial length (Marroig et al. 2009). This suggests not only that Canidae are more able to respond to selective pressure on the relative length of the face, but also that these traits will respond jointly to selection.

This might have played an important role in the evolutionary history of Canidae, mainly for the evolution of hypercarnivory (the consumption of large vertebrates), a transition that has occurred multiple times along the history of the group (Prevosti 2010; Perini et al. 2010; Slater 2015). For canids, a decrease in relative snout length is associated with an increase in both bite forces (Damasceno et al. 2013) and mechanical performance for capturing large prey (Slater et al. 2009), which might explain why hypercarnivores are usually more brachyrostral than generalist species. An increased capacity to change the relative size of the face can thus allow for rapid adaptation in response to changing ecological conditions, such as availability of new food sources or interspecific competition for resources (Van Valkenburgh and Wayne 1994). These changes, however, are usually thought to be decoupled from size evolution (Van Valkenburgh and Wayne 1994; Damasceno et al. 2013), suggesting that the observed differences in integration might facilitate morphological evolution in both size and nonsize (shape) related directions.

The suggestion that Canidae have a high propensity for morphological evolution of facial traits is not new. Laidlaw et al. (2007) demonstrated that Canidae have an elevated incidence of pure repetitive sequences (not interrupted by point mutations), a fact that could increase the capacity of a species to create new variation by duplication (Fondon and Garner 2004; Laidlaw et al. 2007). For example, this is supposedly what happened in the *Runx2* gene for osteoblast differentiation, for which differences in the number of repeated elements in the polyglutaminepolyalanine-rich regions are positively related with facial length in both domestic breeds of dogs (Fondon and Garner 2004, 2007) and Carnivore species (Sears et al. 2007). Thus, the increased evolutionary potential observed here could be associated to differences in the Canidae genome, facilitating evolutionary change of the face under natural and artificial selection.

With the results shown here in mind, it is hard not to think of the possible parallels between the shifts of morphological integration in Canidae and the morphological diversity of the domestic dog *Canis familiaris*. Apart from the extreme variation in size and "soft" morphology (e.g., fur traits, ear, and tail shape), the variation in the relative size of the face is a defining feature of the morphological diversity of dogs. The diversity in skull shape of dogs rivals not only that seen in wild canids (Wayne 1986), but also in Carnivora as a whole (Drake and Klingenberg 2010). The fact that Canidae species have more integrated, flexible, and evolvable facial traits might help to explain why we see such a great diversity of cranial shapes in domestic dogs.

This idea is also reinforced by the fact that the dingo (*C. familiaris dingo*) was found here to be at the extremes of the axes of the matrix-spaces that discriminate Canidae from the remaining Carnivora (Fig. 2). Dingoes are considered to be closely related to dogs, being a living representative of the ancient populations of *C. familiaris* (Crowther et al. 2014; Freedman et al. 2014; Dinets 2015; Wang et al. 2016; Jackson et al. 2017). The fact that dingoes can be seen as possessing an extreme version of the morphological integration structure shared by other Canidae suggests that the domestication process of dogs was carried out taking advantage of these patterns of variation (Drake and Klingenberg 2010; Drake 2011; Geiger et al. 2017). These natural tendencies could then have been intensified through artificial selection (see below), thus explaining the differences in allometry seen between dogs and wolves (Sánchez-Villagra et al. 2017; Wilson 2018).

If our suggestion holds, then the increased emphasis on postnatal organ development seen in domestic dogs could help

explain not only why canids have increased allometric coefficients for cranial traits (Werneburg and Geiger 2017; Wilson 2018), but also why they present relatively larger evolvabilities and flexibilities on those traits. This could be seen as contrary to what was suggested by Porto et al. (2013), who argued that more altricial (i.e., less developed at birth) mammals tend to have more integrated skulls, and thus, less flexible skulls. However, even though Canidae shows low overall integration, it is not particularly distinct from other Carnivoran families in this regard (Fig. 2C). It could be that differences such as the one observed here do not reflect the overall metabolic budget expent during ontogeny, but rather a differential resource allocation. More comparative ontogenetic studies on Carnivoran species would certainly help elucidate this issue.

CAUSES FOR STABILITY AND CHANGE

Here, we have analyzed the evolution of patterns and magnitude of morphological integration in the carnivoran skull. Canidae has been shown to diverge from other families by having higher evolvability and flexibility in facial traits. Nevertheless, morphological integration patterns show low phylogenetic signal and high average clade disparity throughout the evolution of the group, while within-group similarities (in Canidae and non-canid Carnivora) remained high, a fact that might be explained by similar internal stabilizing selection. *Ad hoc* simulations have shown that the observed patterns more closely match those of a two-peak OU-process, reinforcing the notion that stabilizing selection is at play in generating within-group (Canidae/non-canid Carnivora) stability.

While it is therefore reasonable to assume that a difference in stabilizing selection may be responsible for the observed differences (Lande 1980; Cheverud 1984), recent theoretical models have argued that directional selection can play an important role in changing the covariance patterns in **G** (Pavlicev et al. 2011). Simulation analyses broadly confirmed this expectation even under different parametrizations (Melo and Marroig 2015; Jones et al. 2014), and recent empirical works have shown that directional selection can alter patterns of integration in the mammalian skull, both in the lab (Penna et al. 2017) and in the wild (Assis et al. 2016). Melo and Marroig (2015)'s model shows that, for a multivariate system, directional correlational selection ("corridor selection") on a module along with stabilizing selection on the remaining traits increases not only the intramodule correlation in the selected module, but also the variation associated with directions that contrast selected and non-selected modules. This description matches what seems to happen in canids, where the facial region suffers an increase in both correlation and variance, suggesting that directional selection may help explain our results. Given the importance of the relative length of the snout for Canidae ecology, it is easy to see how this could have occurred along the evolution of the group.

Here, however, the association between changes in average morphology and morphological integration was weak, except for a correlated change that supposedly took place at the origin of aquatic taxa (Pinnipedia). While this seems to be contrary to the role of directional selection in changing integration in Canidae, it could be the case that the overall stasis of integration patterns experienced throughout the history of the group (Fig. 3) was enough to erode any signal that could possibly be evaluated through distance matrix comparisons. Furthermore, the direction of selection and its interaction with **G** might be essential to understand how selection can affect variation patterns (Pavlicev et al. 2011; Melo and Marroig 2015; Hopkins et al. 2016; Assis et al. 2016; Penna et al. 2017). The reconstruction of past selection regimes and its association with integration patterns may help elucidate when the changes observed in Canidae came about and why. This approach would also be advantageous to investigate how the land-to-water transition has affected morphological integration along with morphology in mammals, as apparently has happened in Pinnipedia.

Lastly, the fact that dingoes have been shown here to be an extreme case of the pattern of variation seen in Canidae raises questions about the relationship between changes in covariance structure and the evolutionary plasticity of dog breeds (Drake and Klingenberg 2010). It could be the case that the changes seen in the dingo happened before the process of domestication, thus facilitating the evolution of extreme morphologies (Houle et al. 2017). Alternatively, if artificial selection was responsible for the covariation change seen in dingoes (Pavlicev et al. 2011; Walter et al. 2018) then it is remarkable that this change could still be detected in a feral subspecies that has been evolving semi-independently from other dogs for thousands of years. Further investigation into changes in covariation under domestication in dogs could help understand not only how selection can change covariance structures, but also how these changes can then be fixated under natural conditions.

AUTHOR CONTRIBUTIONS

Conceptualization, F.A.M. and G.M.; Data gathering, F.A.M. (Caniformes) and T.M.G.Z. (Feliformes); Investigation, all authors; Computer code, F.A.M.; Resources, G.M.; Writing, all authors; Funding Acquisition, all authors.

ACKNOWLEDGMENTS

We are deeply grateful to people and institutions that provided help and access to zoological collections: Mario de Vivo and Juliana Gualda (Museu de Zoologia da Universidade de São Paulo; São Paulo); Joo João Oliveira, Luiz Flamarion and Sérgio Maia Vaz (Museu Nacional; Rio de Janeiro); David Flores and Sergio Lucero (Museu Argentino de Ciencias Naturales "Bernardino Rivadavia", Buenos Aires); Diego Verzi and Itati Olivares (Museu La Plata, La Plata); Eileen Lacey and Chris Conroy (Museum of Vertebrate Zoology, Berkeley); Nancy B. Simmons, Neil Duncan, Eileen

Westwig, Aja Marcato and Eleanor Hoeger (American Museum of Natural History, New York); Kris Helgen, Darrin Lunde, Esther Langan, and John Ososky (Smithonian Institute, Washington); Bruce Patterson, Bill Stanley (*in memoriam*) (Field Museum, Chicago); Hopi Hoekstra and Judith Chupasko (Museum of Comparative Zoology, Cambridge); Ted Daeschler and Ned Gilmore (Academy of Natural Sciences of Drexel University, Philadelphia); Frieder Mayer and Christiane Funk (Museum für Naturkunde, Berlin); Frank Zachos and Alexander Bibl (Naturhistorisches Museum Wien, Vienna); Graldine Veron (Muséum National d'Histoire Naturelle, Paris); Jan Decher and Christian Montermann (Zoologisches Forschungsmuseum Alexander Koenig, Bonn); Petr Benda (Přírodovědecké muzeum, Národní muzeum, Prague); Robert Asher and Matthew Lowe (University Museum of Zoology, Cambridge); Irina Ruf and Katrin Krohmann (Senckenberg Naturmuseum Frankfurt, Frankfurt am Main); and Pepijn Kamminga (Naturalis Biodiversity Centre, Leiden). This article was supported by scholarships and grants from Fundação de Amparo à Pesquisa do Estado de São Paulo (FAM 2011/21674-4, 2013/22042-7; TMZ 2013/07299-1, 2014/12403-5; GM 2011/14295-7) and Santander. We would like to thank G. Garcia and three anonymous reviewers for insightful comments, Barbara Costa and Daniela Rossoni for productive discussions on phylogenetic comparative methods and James Rohlf for some clarifications on the use of the Random Skewers method. We also would like to thank J. Wolf (University of Bath) and B. Dummont (University of Massachussets-Amherst) for providing support during the international internships of T.M.G.Z. and F.A.M., respectively. The authors declare no conflict of interest.

DATA ARCHIVAL

Data is publicly available on Dryad (https://doi.org/10.5061/dryad.142jn5t).

LITERATURE CITED

Ackermann, R. R., and J. M. Cheverud. 2000. Phenotypic covariance structure in tamarins(genus *Saguinus*): a comparison of variation patterns using matrix correlation and common principal component analysis. Am. J. Phys. Anthropol. 111:489–501.

———. 2004. Detecting genetic drift versus selection in human evolution. Proc. Natl. Acad. Sci. USA 101:17946–17951.

Adams, D. C. 2014. A generalized K statistic for estimating phylogenetic signal from shape and other high-dimensional multivariate data. Syst. Zool. 63:685–697.

Adams, D. C., and E. Otárola-Castillo. 2013. geomorph: an rpackage for the collection and analysis of geometric morphometric shape data. Methods Ecol. Evol. 4:393–399.

Agnarsson, I., M. Kuntner, and L. J. May-Collado. 2010. Dogs, cats, and kin: a molecular species-level phylogeny of Carnivora. Mol. Phylogenet. Evol. 54:726–745.

Agrawal, A. F., and J. R. Stinchcombe. 2009. How much do genetic covariances alter the rate of adaptation? Proc. R Soc. Lond. Ser. B Biol. Sci. 276:1183–1191.

Anderson, M. 2001. A new method for non-parametric multivariate analysis of variance. Austral. Ecol. 26:32–46.

Arnold, C., L. J. Matthews, and C. L. Nunn. 2010. The 10kTrees website: a new online resource for primate phylogeny. Evol. Anthropol. 19:114–118.

Assis, A. P. A., J. L. Patton, A. Hubbe, and G. Marroig. 2016. Directional selection effects on patterns of phenotypic (co)variation in wild populations. Proc. R Soc. Lond. Ser. B Biol. Sci. 283:20161615.

Bininda-Emonds, O. R., M. Cardillo, K. E. Jones, R. D. MacPhee, R. M. Beck, R. Grenyer, S. A. Price, R. A. Vos, J. L. Gittleman, and A. Purvis, 2007. The delayed rise of present-day mammals. Nature 446:507.

Blankers, T., D. A. Gray, and R. M. Hennig, 2017. Multivariate phenotypic evolution: divergent acoustic signals and sexual selection in gryllus field crickets. Evol. Biol. 44:1–13.

Blomberg, S. P., J. Theodore Garland, and A. Ives. 2003. Testing for phylogenetic signal in comparative data: behavioral traits are more labile. Evolution 57:717–745.

Bookstein, F. L., and P. Mitteroecker. 2014. Comparing covariance matrices by relative eigenanalysis, with applications to organismal biology. Evol. Biol. 41:336–350 .

Britton, T., C. L. Anderson, D. Jacquet, S. Lundqvist, and K. Bremer. 2007. Estimating divergence times in large phylogenetic trees. Syst. Biol. 56:741–752.

Cheverud, J. M. 1982. Phenotypic, genetic, and environmental morphological integration in the cranium. Evolution 36:499–516.

———. 1984. Quantitative genetics and developmental constraints on evolution by selection. J. Theoret. Biol. 110:155–171.

———. 1988. A comparison of genetic and phenotypic correlations. Evolution 42:958–968.

———. 1995. Morphological integration in the saddle-back tamarin (*Saguinus fuscicollis*) cranium. Am. Nat. 145:63–89.

———. 1996a. Developmental integration and the evolution of pleiotropy. Integr. Comp. Biol. 36:44–50.

———. 1996b. Quantitative genetic analysis of cranial morphology in the cotton-top (*Saguinus oedipus*) and saddle-back (*S*. fuscicollis) tamarins. J. Evol. Biol. 9:5–42.

Cheverud, J. M., and G. Marroig. 2007. Comparing covariance matrices: random skewers method compared to the common principal components model. Genet. Mol. Biol. 30:461–469.

Cheverud, J. M., J. Rutledge, and W. Atchley. 1983. Quantitative genetics of development: genetic correlations among age-specific trait values and the evolution of ontogeny. Evolution 37:895–905.

Christiansen, P. 2008. Evolutionary changes in craniomandibular shape in the great cats (*Neofelis* Griffith and *Panthera* Oken). Biol. J. Linnean Soc. 95:766–778.

Crowther, M. S., M. Fillios, N. Colman, and M. Letnic. 2014. An updated description of the Australian dingo (*Canis dingo*Meyer, 1793). J. Zool. 293:192–203.

Cuvier, G., and R. Jameson. 1827. Essay on the theory of the earth. W. Blackwood, Edinburgh, U.K.

Damasceno, E. M., E. Hingst-Zaher, and D. Astúa, 2013. Bite force and encephalization in the Canidae (Mammalia: Carnivora). J. Zool. 290:246–254.

Darwin, C. 1859. On the origin of species by means of natural selection. John Murray, London.

Dayan, T., D. Wool, and D. Simberloff, 2002. Variation and covariation of skulls and teeth: modern carnivores and the interpretation of fossil mammals. Paleobiology 28:508–526.

Dinets, V. 2015. The *Canis* tangle: a systematics overview and taxonomic recommendations. Vavilovskii Zhurnal Genetiki i Selektsii Vavilov J. Genet. Breeding 19:286–291.

Dow, M., and J. M. Cheverud. 1985. Comparison of distance matrices in studies of population structure and genetic microdifferentiation: quadratic assignment. Am. J. Phys. Anthropol. 63:367–373.

Drake, A. G. 2011. Dispelling dog dogma: an investigation of heterochrony in dogs using 3D geometric morphometric analysis of skull shape. Evol. Dev. 13:204–213.

Drake, A. G., and C. P. Klingenberg. 2010. Large-scale diversification of skull shape in domestic dogs: disparity and mod. 175:289–300.

Dryden, I. L., A. Koloydenko, and D. Zhou, 2009. Non-Euclidean statistics for covariance matrices, with applications to diffusion tensor imaging. Annal. Appl. Stat. 3:1102–1123.

Dumont, M., C. E. Wall, L. Botton Divet, A. Goswami, S. Peigné, and A.-C. Fabre, 2016. Do functional demands associated with locomotor habitat, diet, and activity pattern drive skull shape evolution in musteloid carnivorans? Biol. J. Linnean Soc. 117:858–878.

Eastman, J. M., L. J. Harmon, and D. C. Tank, 2013. Congruification: support for time scaling large phylogenetic trees. Methods Ecol. Evol. 4:688–691.

Edwards, D. L., J. Melville, L. Joseph, and J. S. Keogh. 2015. Ecological divergence, adaptive diversification, and the evolution of social signaling traits: an empirical study in arid Australian lizards. Am. Nat. 186:E144–E161.

Falconer, D. S., T. F. Mackay, and R. Frankham. 1996. Introduction to quantitative genetics (4th edn). Trends Genet. 12:280.

Felsenstein, J. 2004. Inferring phylogenies, vol. 2. Sinauer associates, Sunderland.

Figueirido, B., N. MacLeod, J. Krieger, M. D. Renzi, J. Perez-Claros, and P. Palmqvist, 2011a. Constraint and adaptation in the evolution of carnivoran skull shape. Paleobiology 37:490–518.

Figueirido, B., P. Palmqvist, and J. A. Pérez-Claros, 2009. Ecomorphological correlates of craniodental variation in bears and paleobiological implications for extinct taxa: an approach based on geometric morphometrics. J. Zool. 277:70–80.

Figueirido, B., F. J. Serrano-Alarcón, and P. Palmqvist. 2011b. Geometric morphometrics shows differences and similarities in skull shape between the red and giant pandas. J. Zool. 286:293–302.

Figueirido, B., F. J. Serrano-Alarcón, G. J. Slater, and P. Palmqvist. 2010. Shape at the cross-roads: homoplasy and history in the evolution of the carnivoran skull towards herbivory. J. Evol. Biol. 23:2579–2594.

Figueirido, B., Z. J. Tseng, and A. Martín-Serra, 2013. Skull shape evolution in durophagous carnivorans. Evolution 67:1975–1993.

Figueiró, H. V., G. Li, F. J. Trindade, J. Assis, F. Pais, G. Fernandes, S. H. D. Santos, G. M. Hughes, A. Komissarov, A. Antunes, et al. 2017. Genome-wide signatures of complex introgression and adaptive evolution in the big cats. Sci. Adv. 3:e1700299.

Fondon, J., and H. Garner. 2004. Molecular origins of rapid and continuous morphological evolution. Proc. Natl. Acad. Sci. USA 101:18058–18063.

———. 2007. Detection of length-dependent effects of tandem repeat alleles by 3-D geometric decomposition of craniofacial variation. Dev. Genes Evol. 217:79–85.

Förstner, W., and B. Moonen. 1999. A metric for covariance matrices. Pp. 113–128 *in* Quo vadis geode sia..., Festschrift for Erik W. Grafarend on the occasion of his th birthday. Geodesy-The Challenge of the 3rd Millennium.

Freedman, A. H., I. Gronau, R. M. Schweizer, D. Ortega-Del Vecchyo, E. Han, P. M. Silva, M. Galaverni, Z. Fan, P. Marx, B. Lorente-Galdos, et al. 2014. Genome sequencing highlights the dynamic early history of dogs. PLoS Genet. 10:e1004016.

Garcia, G. R. G., E. Hingst-Zaher, R. Cerqueira, and G. Marroig. 2014. Quantitative genetics and modularity in cranial and mandibular morphology of calomys expulsus. Evol. Biol. 41:619–636.

Garcia, G. R. G., F. B. d. Oliveira, and G. Marroig. 2016. A phylogenetic analysis of shape covariance structure in the anthropoid skull. 1–38.

Gaubert, P., W. C. Wozencraft, P. Cordeiro-Estrela, and G. Veron. 2005. Mosaics of convergences and noise in Morphological Phylogenies: What's in a Viverrid-Like Carnivoran? Syst. Zool. 54:865–894.

Geiger, M., A. Evin, M. R. S. x. nchez Villagra, D. Gascho, C. Mainini, and C. P. E. Zollikofer. 2017. Neomorphosis and heterochrony of skull shape in dog domestication. Sci. Rep. 7:1–9.

Goswami, A. 2006a. Cranial modularity shifts during mammalian evolution. Am. Nat. 168:270.

———. 2006b. Morphological integration in the carnivoran skull. Evolution 60:169–183.

———. 2010. Introduction to carnivora. Chap. 1, *in* A. Goswami, and A. Friscia, eds. Carnivoran evolution. New views on phylogeny, form and function. Cambridge Univ. Press, Cambridge.

Grabowski, M. 2016. Bigger brains led to bigger bodies?: the correlated evolution of human brain and body size. Curr. Anthropol. 57:174–196.

Haber, A. 2015. The evolution of morphological integration in the ruminant skull. Evol. Biol. 42:99–114.

———. 2016. Phenotypic covariation and morphological diversification in the ruminant skull. Am. Nat. 187:576–591.

Hall, B. K. 2005. Bones and cartilage: developmental and evolutionary skeletal biology. Elsevier Academic Press, San Diego, CA.

Hallgrímsson, B., H. Jamniczky, N. Young, C. Rolian, T. Parsons, J. Boughner, and R. S. Marcucio. 2009. Deciphering the palimpsest: studying the relationship between morphological integration and phenotypic covariation. Evol. Biol. 36:355–376.

Hallgrímsson, B., D. Lieberman, N. Young, T. Parsons, and S. Wat. 2007. Evolution of covariance in the mammalian skull. Pp. 164–190 *in* Novartis Foundation Symposium. John Wiley, Chichester, New York.

Hansen, T. 1997. Stabilizing selection and the comparative analysis of adaptation. Evolution 51:1341–1351.

———. 2006. The evolution of genetic architecture. Ann. Rev. Ecol. Evol. Syst. 37:123–157.

Hansen, T., and D. Houle. 2008. Measuring and comparing evolvability and constraint in multivariate characters. J. Evol. Biol. 21:1201–1219.

Hansen, T. F., and E. Martins. 1996. Translating between microevolutionary process and macroevolutionary patterns: the correlation structure of interspecific data. Evolution 50:1404–1417.

Harmon, L. J., and R. E. Glor. 2010. Poor statistical performance of the Mantel test in phylogenetic comparative analyses. Evolution 64:2173–2178.

Harmon, L. J., J. A. Schulte, A. Larson, and J. B. Losos. 2003. Tempo and mode of evolutionary radiation in iguanian lizards. Science 301:961–964.

Harmon, L. J., J. T. Weir, C. D. Brock, R. E. Glor, and W. Challenger. 2007. GEIGER: investigating evolutionary radiations. Bioinformatics 24:129–131.

Hervé, M. 2016. RVAideMemoire: diverse basic statistical and graphical functions. R package version 0.9–55.

Hopkins, M. J., A. Haber, and C. L. Thurman. 2016. Constraints on geographic variation in fiddler crabs (Ocypodidae: Uca) from the western Atlantic. J. Evol. Biol. 29:1553–1568.

Houle, D., G. H. Bolstad, K.van der Linde, and T. F. Hansen. 2017. Mutation predicts 40 million years of fly wing evolution. Nature 143:1–16.

Hubbe, A., D. Melo, and G. Marroig. 2016. A case study of extant and extinct *Xenarthra cranium* covariance structure: implications and applications to paleontology. Paleobiology 42:465–488.

Jackson, S. M., C. P. Groves, P. J. S. Fleming, K. P. Aplin, M. D. B. Eldridge, A. Gonzales, and K. M. Helgen. 2017. The wayward dog: is the Australian native dog or Dingo a distinct species? Zootaxa 4317:201–24.

Jolicoeur, P. 1963. The multivariate generalization of the allometry equation. Biometrics 19:497–499.

Jones, A. G., R. Bürger, and S. J. Arnold. 2014. Epistasis and natural selection shape the mutational architecture of complex traits. Nat. Comm. 5:3709.

Jones, K. E., and A. Goswami. 2009. Quantitative analysis of the influences of phylogeny and ecology on phocid and otariid pinniped (Mammalia; Carnivora) cranial morphology. J. Zool. 280:297–308.

Jones, K. E., J. B. Smaers, and A. Goswami. 2015. Impact of the terrestrial-aquatic transition on disparity and rates of evolution in the carnivoran skull. BMC Evol. Biol. 15:1–19.

Kienle, S. S., and A. Berta. 2015. The better to eat you with: the comparative feeding morphology of phocid seals (Pinnipedia, Phocidae). J. Anat. 228:396–413.

Laidlaw, J., Y. Gelfand, K. W. Ng, H. R. Garner, R. Ranganathan, G. Benson, and J. W. Fondon. 2007. Elevated basal slippage mutation rates among the Canidae. J. Heredity 98:452–460.

Lande, R. 1979. Quantitative genetic analysis of multivariate evolution, applied to brain: body size allometry. Evolution 33:402–416.

———. 1980. The genetic covariance between characters maintained by pleiotropic mutations. Genetica 94:203–215.

Lande, R., and S. J. Arnold. 1983. The measurement of selection on correlated characters. Evolution 37:1210–1226.

Lessells, C. M., and P. T. Boag. 1987. Unrepeatable repeatabilities: a common mistake. The Auk 104:116–121.

Li, G., B. Davis, E. Eizirik, and W. J. Murphy. 2015. Phylogenomic evidence for ancient hybridization in the genomes of living cats (Felidae). Genome Res. P. gr.186668.114.

Lynch, M., B. Walsh, 1998. Genetics and analysis of quantitative traits, vol. 1. Sinauer Sunderland, MA.

Lysy, M., A. D. Stasko, and H. K. Swanson, 2014. nicheROVER: (Niche) (R)egion and Niche (Over)lap metrics for multidimensional ecological niches. R package version 1.0.

Mantel, N. 1967. The detection of disease clustering and a generalized regression approach. Cancer Res. 27:209–220.

Marroig, G., and J. M. Cheverud. 2001. A comparison of phenotypic variation and covariation patterns and the role of phylogeny, ecology, and ontogeny during cranial evolution of New World monkeys. Evolution 55:2576–2600.

———. 2005. Size as a line of least evolutionary resistance: diet and adaptive morphological radiation in new world monkeys. Evolution 59:1128–1142.

———. 2010. Size as a line of least resistance II: direct selection on size or correlated response due to constraints? Evolution 64:1470–1488.

Marroig, G., D. Melo, A. Porto, H. Sebastião, and G. R. G. Garcia. 2011. Selection response decomposition (SRD): a new tool for dissecting differences and similarities between matrices. Evol. Biol. 38:225–241.

Marroig, G., D. A. R. Melo, and G. R. G. Garcia. 2012. Modularity, noise, and natural selection. Evolution 66:1506–1524.

Marroig, G., L. T. Shirai, A. Porto, F. B. d. Oliveira, and V. Conto. 2009. The evolution of modularity in the mammalian skull II: evolutionary consequences. Evol. Biol. 36:136–148.

Marroig, G., M. Vivo, and J. M. Cheverud. 2004. Cranial evolution in sakis (Pithecia, Platyrrhini) II: evolutionary processes and morphological integration. J. Evol. Biol. 17:144–155.

Martínez-Abadías, N., M. Esparza, T. Sjøvold, R. González-José, M. Santos, M. Hernández, and C. P. Klingenberg. 2012. Pervasive genetic integration directs the evolution of human skull shape. Evolution 66:1010–1023.

Mattson, D. J. 1998. Diet and morphology of extant and recently extinct northern bears. Ursus 10:479–496.

McArdle, B., and M. Anderson. 2001. Fitting multivariate models to community data: a comment on distance-based redundancy analysis. Ecology 82:290–297.

Meiri, S., T. Dayan, and D. Simberloff. 2005. Variability and correlations in carnivore crania and dentition. Funct. Ecol. 19:337–343.

Melo, D., and G. Marroig. 2015. Directional selection can drive the evolution of modularity in complex traits. Proc. Natl. Acad. Sci. USA 112:470–475.

Meloro, C., M. Clauss, and P. Raia. 2015. Ecomorphology of carnivora challenges convergent evolution. Org. Diver. Evol. 15:711–720.

Meloro, C., A. Hudson, and L. Rook, 2014. Feeding habits of extant and fossil canids as determined by their skull geometry. J. Zool. 295:178–188.

Michaud, M., G. Veron, S. Peigné, A. Blin, and A.-C. Fabre. 2018. Are phenotypic disparity and rate of morphological evolution correlated with ecological diversity in Carnivora? Bio. J. Linnean Soc. Early view. 1–14.

Mitteroecker, P., and F. Bookstein. 2009. The ontogenetic trajectory of the phenotypic covariance matrix, with examples from craniofacial shape in rats and humans. Evolution 63:727–737.

Nyakatura, K., and O. R. P. Bininda-Emonds. 2012. Updating the evolutionary history of Carnivora (Mammalia): a new species-level supertree complete with divergence time estimates. BMC Biol. 10:1–31.

Oliveira, F. B. d., A. Porto, and G. Marroig. 2009. Covariance structure in the skull of Catarrhini: a case of pattern stasis and magnitude evolution. J. Hum. Evol. 56:417–430.

Olson, E. C., and R. L. Miller, 1958. Morphological integration. Chicago Univ. Press, Chicago and London.

Pavlicev, M., E. A. Norgard, G. L. Fawcett, and J. M. Cheverud. 2011. Evolution of pleiotropy: epistatic interaction pattern supports a mechanistic model underlying variation in genotype-phenotype map. J. Exp. Zool. Part B 316B:371–385.

Pavoine, S., M. Baguette, and M. B. Bonsall. 2010. Decomposition of trait diversity among the nodes of a phylogenetic tree. Ecol. Monogr. 80:485–507.

Pearson, K., and A. G. Davin. 1924. On the biometric constants of the human skull. Biometrika 16:328–363.

Penna, A., D. Melo, S. Bernardi, M. I. Oyarzabal, and G. Marroig. 2017. The evolution of phenotypic integration: how directional selection reshapes covariation in mice. Evolution 71:2370–2380.

Perini, F., C. A. Russo, and C. Schrago. 2010. The evolution of South American endemic canids: a history of rapid diversification and morphological parallelism. J. Evol. Biol. 23:311–322.

Porto, A., F. B. d. Oliveira, L. T. Shirai, V. Conto, and G. Marroig. 2009. The evolution of modularity in the mammalian skull I: morphological integration patterns and magnitudes. Evol. Biol. 36:118–135.

Porto, A., H. Sebastião, S. E. Pavan, J. L. VandeBerg, G. Marroig, and J. M. Cheverud, 2015. Rate of evolutionary change in cranial morphology of the marsupial genus *Monodelphisis* constrained by the availability of additive genetic variation. J. Evol. Biol. 28:973–985.

Porto, A., L. T. Shirai, F. B. d. Oliveira, and G. Marroig. 2013. Size variation, growth strategies, and the evolution of modularity in the mammalian skull. Evolution 67:3305–3322.

Prevosti, F. J. 2010. Phylogeny of the large extinct South American Canids (Mammalia, Carnivora, Canidae) using a "total evidence" approach. Cladistics 26:456–481.

Radinsky, L. B. 1981a. Evolution of skull shape in carnivores: 1. Representative modern carnivores. Biol. J. Linnean Soc. 15:369–388.

———. 1981b. Evolution of skull shape in carnivores: 2. Additional modern carnivores. Biol. J. Linnean Soc. 16:337–355.

———. 1982. Evolution of skull shape in carnivores; 3, The origin and early radiation of the modern carnivore families. Paleobiology 8:177–195.

Rohlf, F. J. 2017. The method of random skewers. Evol. Biol. 44:542–550.

Sacco, T., and B. Van Valkenburgh. 2004. Ecomorphological indicators of feeding behaviour in the bears (Carnivora: Ursidae). J. Zool. 263:41–54.

Sánchez-Villagra, M. R., V. Segura, M. Geiger, L. Heck, K. Veitschegger, and D. Flores. 2017. On the lack of a universal pattern associated with mammalian domestication: differences in skull growth trajectories across phylogeny. R Soc. Open Sci. 4:170876–170812.

Savell, K. R. R., B. M. Auerbach, and C. C. Roseman. 2016. Constraint, natural selection, and the evolution of human body form. Proc. Natl. Acad. Sci. USA 113:9492–9497.

Schoch, R. R. 2006. Skull ontogeny: developmental patterns of fishes conserved across major tetrapod clades. Evol. Dev. 8:524–536.

Schönemann, P. H. 1966. A generalized solution of the orthogonal procrustes problem. Psychometrika 31:1–10.

Schroeder, L., C. C. Roseman, J. M. Cheverud, and R. R. Ackermann. 2014. Characterizing the evolutionary path(s) to early *homo*. PLOS ONE 9:e114307.

Sears, K., A. Goswami, J. Flynn, and L. Niswander. 2007. The correlated evolution of Runx2 tandem repeats, transcriptional activity, and facial length in Carnivora. Evol. Dev. 9:555–565.

Shirai, L. T., and G. Marroig. 2010a. Skull modularity in neotropical marsupials and monkeys: size variation and evolutionary constraint and flexibility. J. Exp. Zool. Part B 314B:663–683.

———. 2010b. Skull modularity in neotropical marsupials and monkeys: size variation and evolutionary constraint and flexibility. J. Exp. Zool. Part B 314:663–683.

Simon, M. N., F. A. Machado, and G. Marroig. 2016. High evolutionary constraints limited adaptive responses to past climate changes in toad skulls. Proc. R Soc. Lond. Ser. B Biol. Sci. 283:1–10.

Slater, G. J. 2015. Iterative adaptive radiations of fossil canids show no evidence for diversity-dependent trait evolution. Proc. Natl. Acad. Sci. USA 112:4897–4902.

Slater, G. J., E. R. Dumont, and B. Van Valkenburgh. 2009. Implications of predatory specialization for cranial form and function in canids. J. Zool. 278:181–188.

Slater, G. J., B. Figueirido, L. Louis, P. Yang, and B. Van Valkenburgh. 2010a. Biomechanical consequences of rapid evolution in the polar bear lineage. PLOS ONE 5:e13870.

Slater, G. J., L. J. Harmon, and M. E. Alfaro. 2012. Integrating fossils with molecular phylogenies improves inference of trait evolution. Evolution 66:3931–3944.

Slater, G. J., S. A. Price, F. Santini, and M. E. Alfaro. 2010b. Diversity versus disparity and the radiation of modern cetaceans. Proc. R. Soc. Lond. Ser. B Biol. Sci. 277:3097–3104.

Steppan, S. 1997. Phylogenetic analysis of phenotypic covariance structure. I. Contrasting results from matrix correlation and common principal component analysis. Evolution 51:571–586.

Strauss, R. E. 2010. Discriminating groups of organisms. Pp. 73–91 *in* Morphometrics for nonmorphometricians. Springer Berlin Heidelberg, Berlin, Heidelberg.

Swanson, H. K., M. Lysy, M. Power, A. D. Stasko, J. D. Johnson, and J. D. Reist, 2015. A new probabilistic method for quantifying n-dimensional ecological niches and niche overlap. Ecology 96:318–324.

Tseng, Z. J., and J. J. Flynn. 2015. An integrative method for testing form-function linkages and reconstructed evolutionary pathways of masticatory specialization. J. R. Soc. Interface 12:1–10.

Tseng, Z. J., and X. Wang. 2011. Do convergent ecomorphs evolve through convergent morphological pathways? Cranial shape evolution in fossil hyaenids and borophagine canids (Carnivora, Mammalia). Paleobiology 37:470–489.

Turelli, M. 1988. Phenotypic evolution, constant covariances, and the maintenance of additive variance. Evolution 42:1342–1347.

Van Valkenburgh, B., and R. K. Wayne. 1994. Shape divergence associated with size convergence in sympatric East African jackals. Ecology 75:1567–1581.

Walter, G. M., J. D. Aguirre, M. W. Blows, and D. Ortiz-Barrientos. 2018. Evolution of genetic variance during adaptive radiation. Am. Nat. 191:E108–E128.

Wang, G.-D., W. Zhai, H.-C. Yang, L. Wang, L. Zhong, Y.-H. Liu, R.-X. Fan, T.-T. Yin, C.-L. Zhu, A. D. Poyarkov, et al. 2016. Out of southern East Asia: the natural history of domestic dogs across the world. Cell Res. 26:21–33.

Wayne, R. 1986. Cranial morphology of domestic and wild canids: the influence of development on morphological change. Evolution 40:243–261.

Werneburg, I., and M. Geiger. 2017. Ontogeny of domestic dogs and the developmental foundations of carnivoran domestication. J. Mammalian Evol. 24:323–343.

Wilson, L. A. B. 2018. The evolution of ontogenetic allometric trajectories in mammalian domestication. Evolution 72:867–877.

Wroe, S., and N. Milne. 2007. Convergence and remarkably consistent constraint in the evolution of carnivore skull shape. Evolution 61:1251–1260.

Zhou, Y., S.-R. Wang, and J.-Z. Ma. 2017. Comprehensive species set revealing the phylogeny and biogeography of Feliformia (Mammalia, Carnivora) based on mitochondrial DNA. PLOS ONE 12:e0174902–19.

Associate Editor: M. Zelditch
Handling Editor: P. Tiffin

Supporting Information

Additional supporting information may be found online in the Supporting Information section at the end of the article.

Figure S1. Example of the impact of differences in group averages in the estimate of the covariance matrix.
Figure S2. Rarefaction analysis of matrix repeatabilities estimated through Monte Carlo and Bootstrap approaches on the *Canis lupus* sample.
Figure S3. Empirical matrix repeatabilities for all species with $n > 5$.
Figure S4. Analysis of rarefaction on the *Canis lupus* sample.
Figure S5. Distribution of cosines of angles between response vectors produced under the Random Skewers framework.
Figure S6. Distribution of angles between response vectors of two matrices
Figure S7. Correlations and trend lines between average RS value and other parameters of the distribution of cosines of angles between response vectors.
Figure S8. Heat map representing pairwise Random Skewers comparisons.
Figure S9. Distribution of the eigenvalues of the Principal Coordinate Analyses of both Dis_{Ri} (A) and Dis_{RS} (B).
Figure S10. Changes along the PCoord axis most aligned with $\sqrt{\bar{r}^2}$ on the space defined by DisRS (PCoord2), as revealed by correlation analysis.
Figure S11. Changes along the PCoord axis most aligned with $\sqrt{\bar{r}^2}$ on the space defined by Dis_{Ri} (PCoord1), as revealed by correlation analysis.
Figure S12. Relationship between within-module average correlation (AVG+) and $\bar{r}^2$ for different cranial modules and regions.
Figure S13. Relationship between among-module average correlation (AVG–) and $\bar{r}^2$ for different cranial modules and regions.
Figure S14. Dated phylogenetic tree used in the comparative analyses.
Figure S15. Results of the diversity decomposition analysis performed on Bininda-Emonds et al. (2007)'s supertree.
Figure S16. Results of the diversity decomposition analysis performed on Nyakatura and Bininda-Emonds (2012)'s supertree.
Figure S17. Results of the diversity decomposition analysis performed on Arnold et al. (2010)'s chronogram.
Figure S18. Simulation of Disparity Through Time following different evolutionary models.
Table S1. Cranial measurements used in the present study.
Table S2. Sample sizes and factors controlled for each species analysed.
Table S3. Repeatability per trait.
Table S4. Results from correlation analyses between PCOA axes and integration measures (overall integration index - $\sqrt{\bar{r}^2}$ - and AVG ratios of the different modularity/region hypotheses).
Table S5. Results from correlation analyses between PCOA axes and trait evolvabilities.
Table S6. Results from correlation analyses between PCOA axes and trait flexibilities.
Table S7. Results from correlation analyses between PCOA axes and allometric coefficients.
Table S8. Modularity tests performed on functional matrix hypotheses.